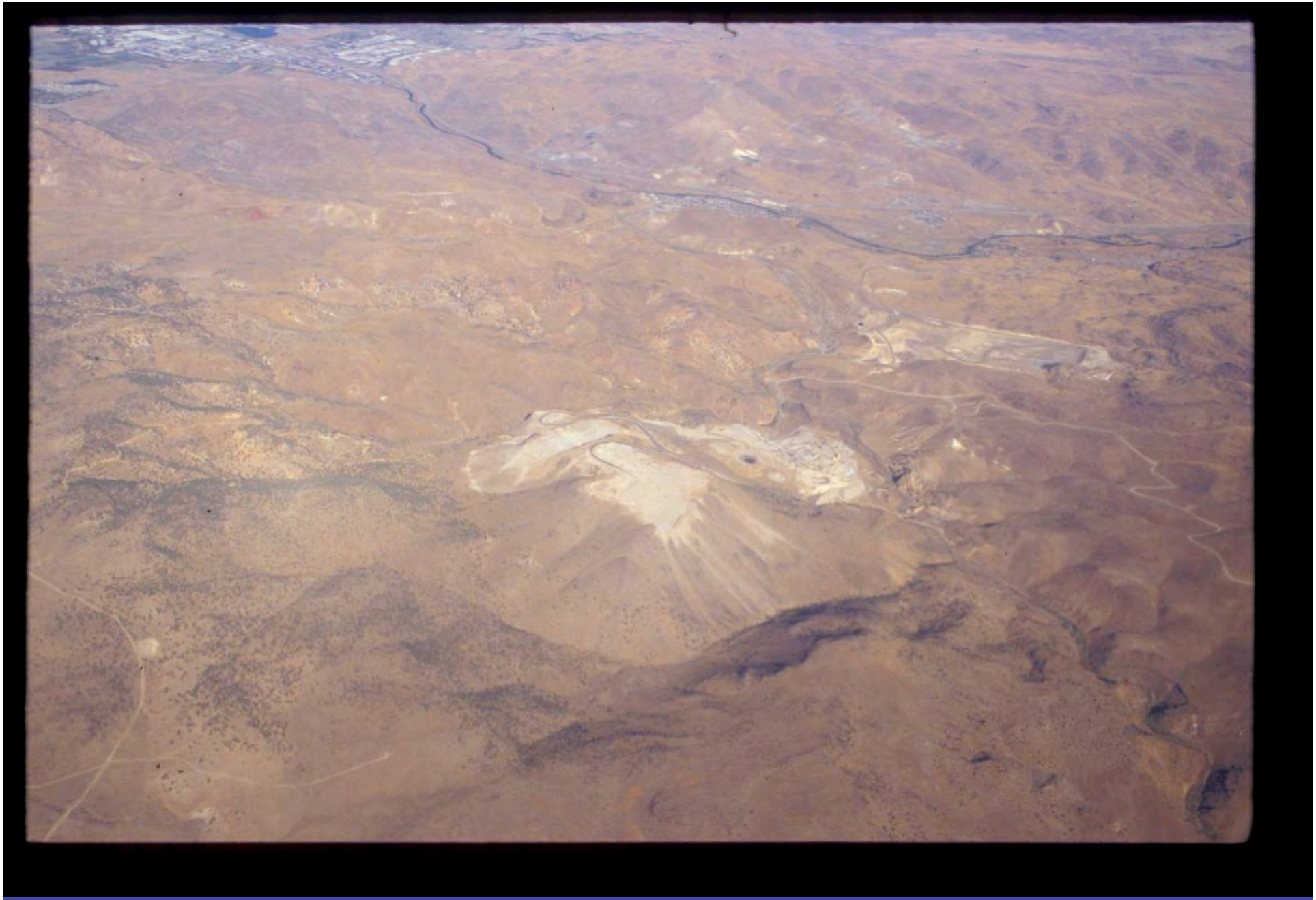

The Carlin gold trend, north central Nevada

Henry & Faulds 2010

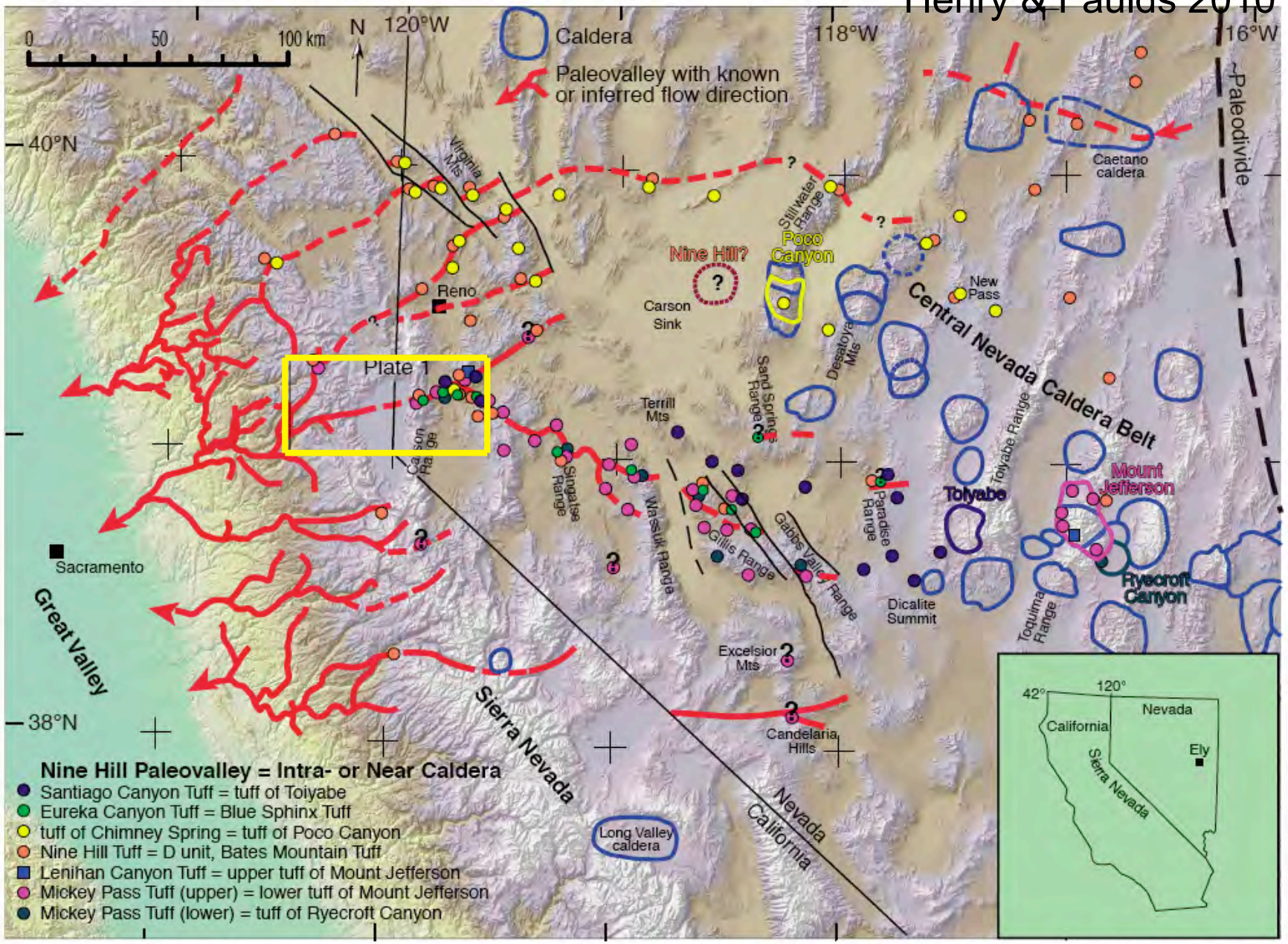

Figure 1. Digital elevation map of the western Great Basin showing the distribution of known paleovalleys and a few segments (from Lindgren, 1911; Jenkins, 1932; Faulds et al., 2005a, 2005b; Garside et al., 2005; this study), a proposed paleodivide (Henry, 2008), known locations of tuffs of the Nine Hill paleovalley (locations with ? are uncertain correlations), and known or suspected calderas for six of the paleovalley tuffs. The paleovalley system drained to the Pacific Ocean, in the Great Valley at the time. The discontinuously exposed paleovalleys in western Nevada probably were more irregular than shown, similar to those in the Sierra Nevada, which are continuously exposed and were mapped in detail.

Henry & Faulds 2010

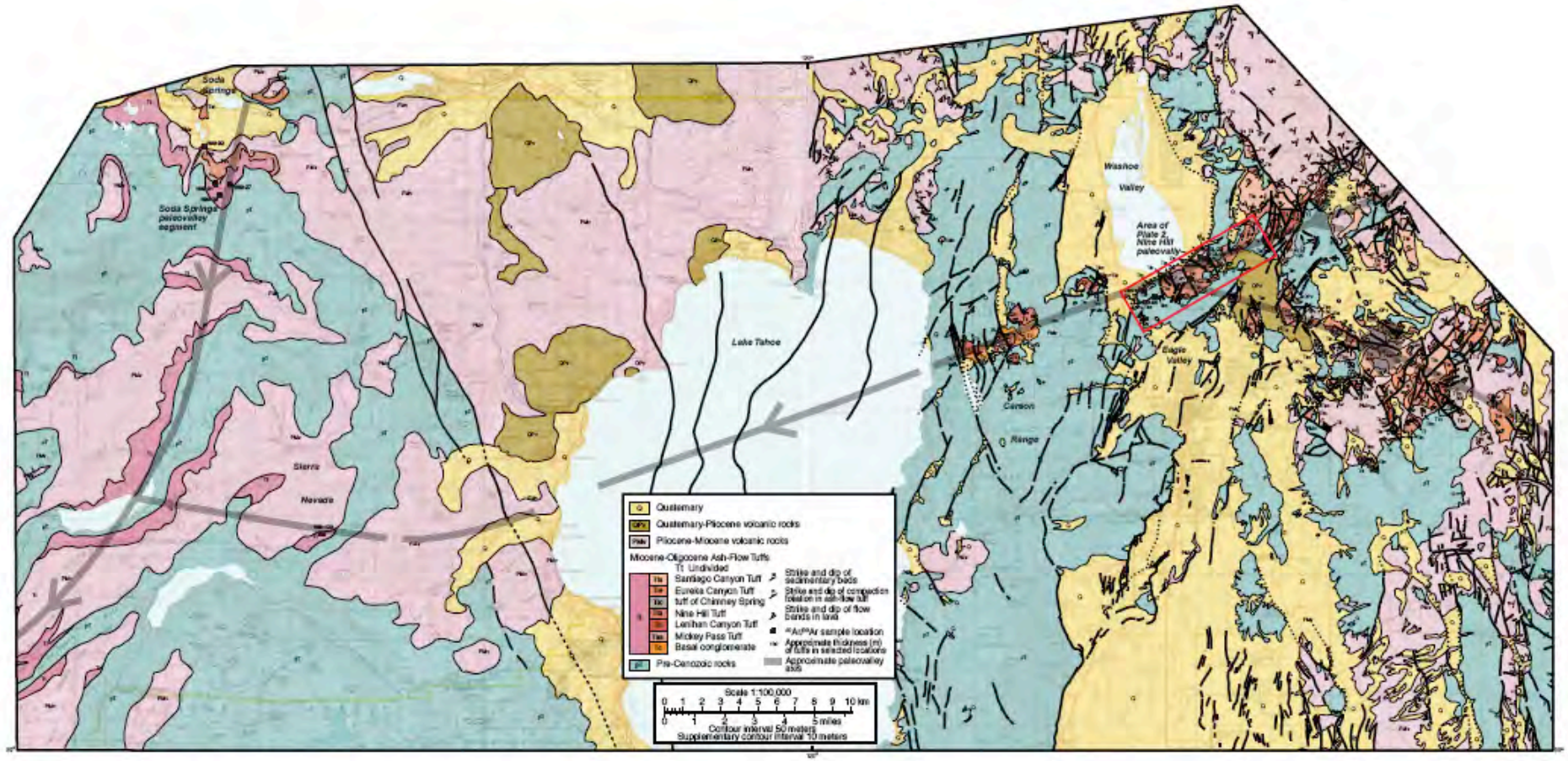

Plate 1. Geology of the region around the Nine Hill paleovalley from Saucedo and Wagner (1992), Stewart (1999), Saucedo (2005), Garside et al. (2005), and this study. If you are

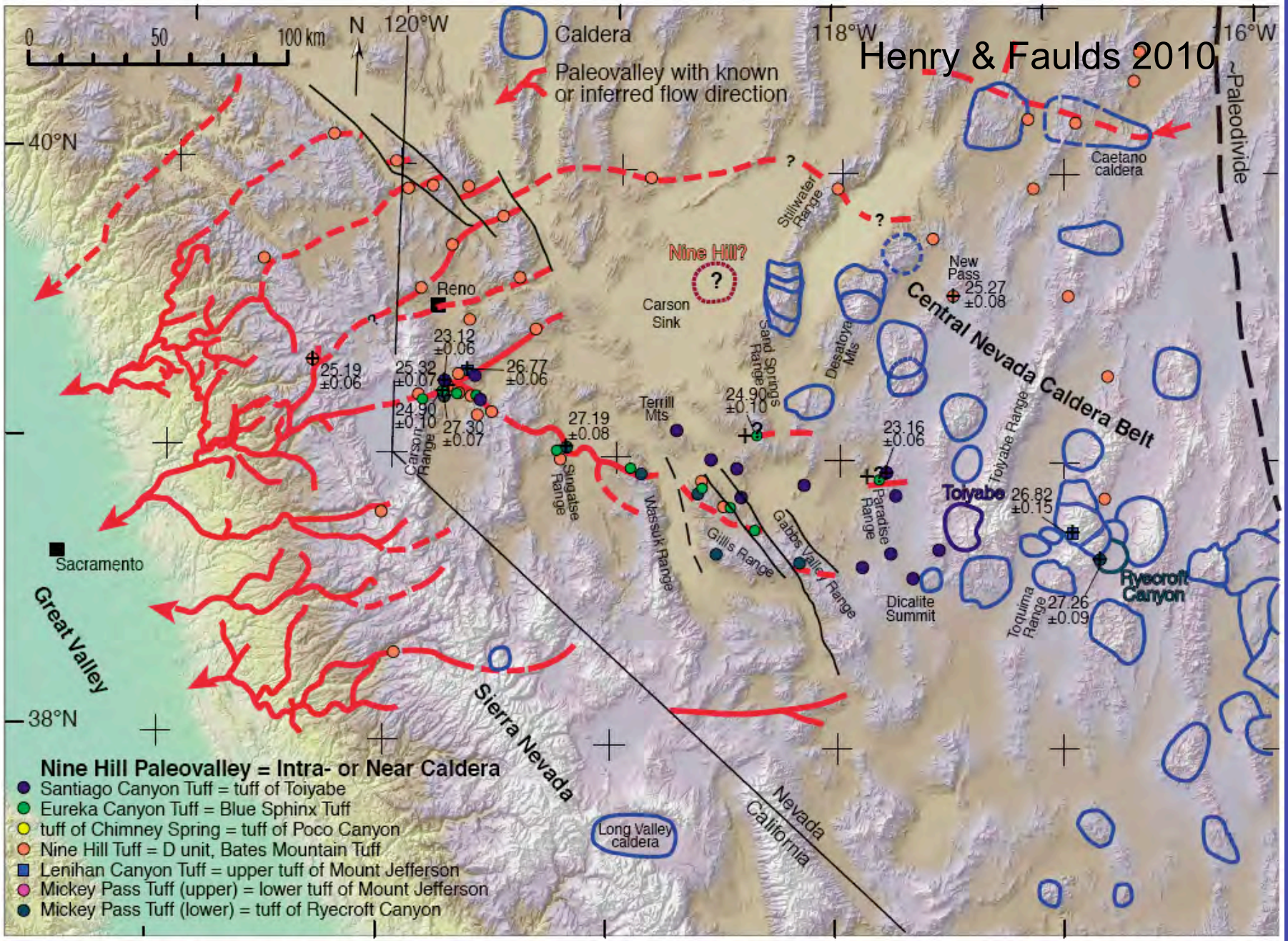

Figure 5. Distribution and ages of the 27.3 Ma Mickey Pass Tuff and correlative tuff of Ryecroft Canyon (source caldera in the Toquima Range), the Lenihan Canyon Tuff and correlative upper tuff of Mount Jefferson, the Nine Hill Tuff (possible source caldera beneath Carson Sink; Deino, 1989), the Eureka Canyon Tuff and correlative Blue Sphinx Tuff, and the Santiago Canyon Tuff and correlative tuff of Toiyabe (source caldera in the Toiyabe Range).

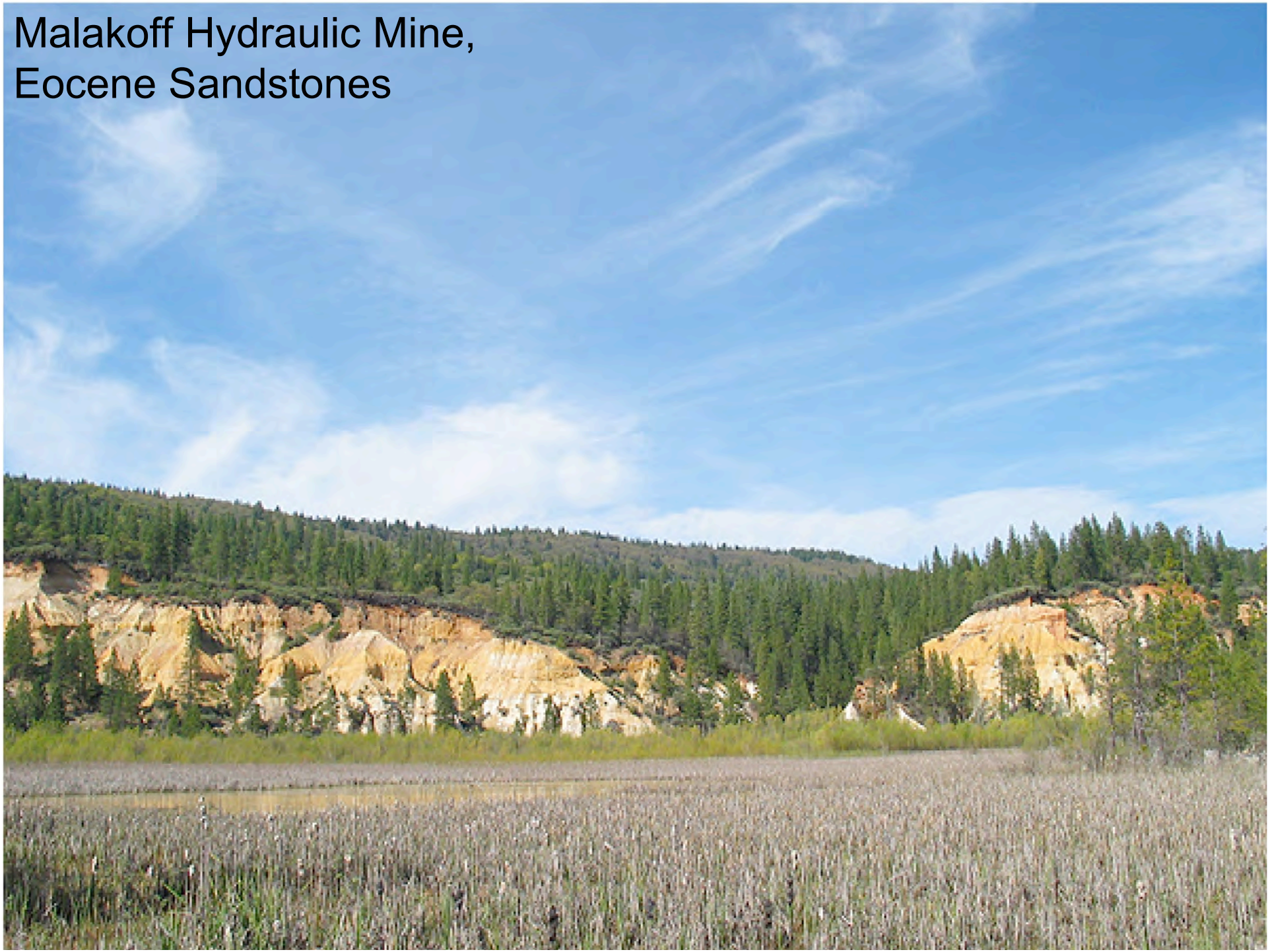
Malakoff Hydraulic Mine,
Eocene Sandstones

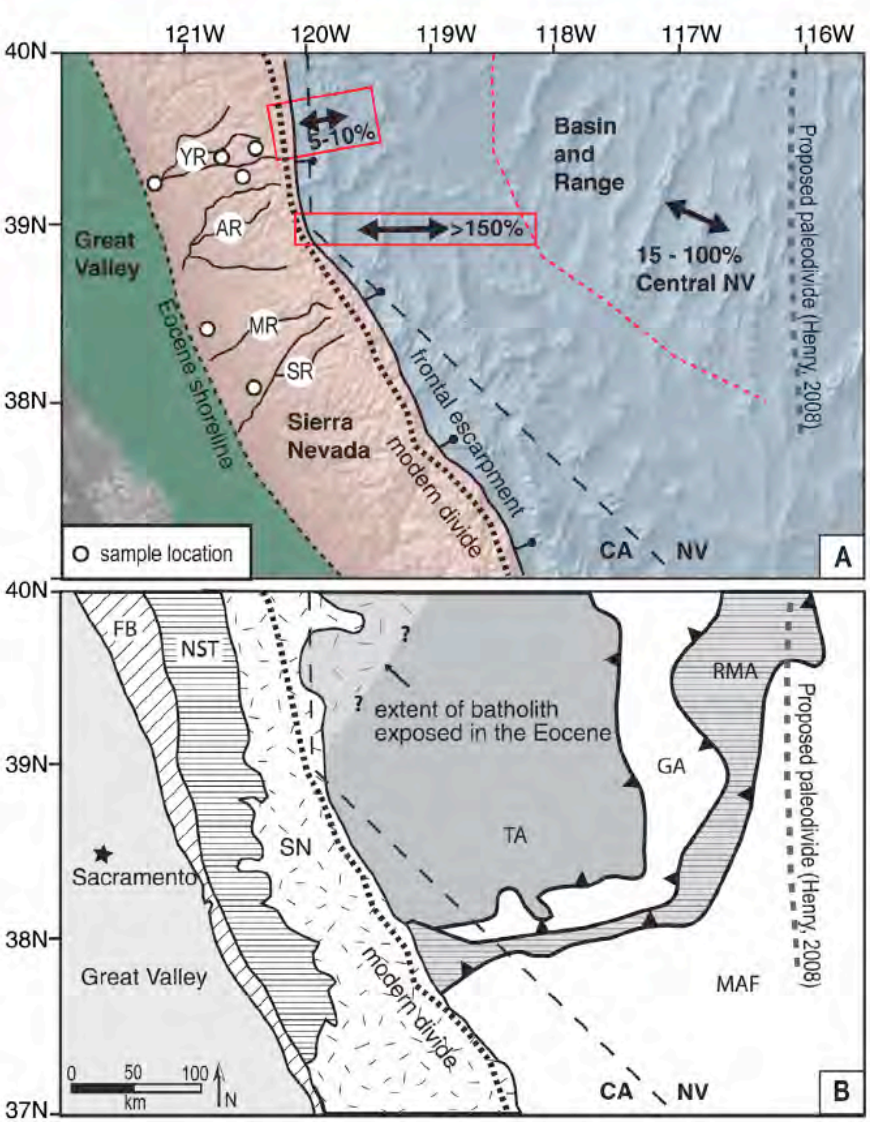

Figure 1. (a) Digital elevation model of the Sierra Nevada and west central Nevada showing present-day topography and location of the modern drainage divide. Sample locations are shown, and major modern rivers discussed in text are outlined. AM, American River; MR, Mokelumne River; SR, Stanislaus River; YR, Yuba River. Mapped Tertiary extension in Nevada is modified after *Van Buer et al.* [2009] and *Cassel et al.* [2009b], and extension estimates are from *Smith et al.* [1991], *Surpless et al.* [2002], and *Faulds et al.* [2005]. (b) Generalized geologic basement map of the same area, showing source terranes and assemblages and their associated boundaries. Map modified after *Gehrels and Miller* [2000]. Location of proposed paleodivide is from *Henry* [2008]. FB, Foothills belt; GA, Golconda allochthon; MAF, Miogeocline and Antler foreland basin strata; NST, northern Sierra terrane; RMA, Roberts Mountain allochthon; SN, Sierra Nevada batholith; TA, Triassic assemblages.

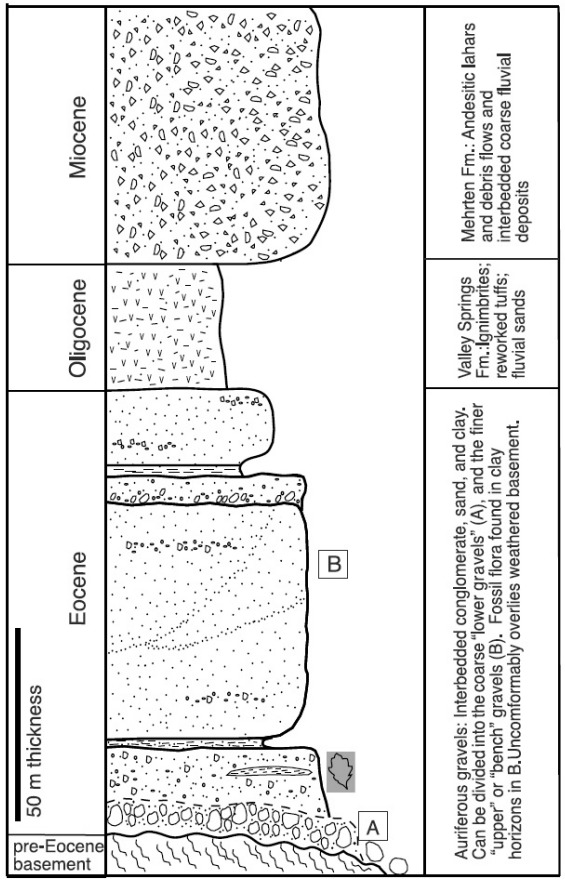

Figure 2. Generalized stratigraphic column for fluvial and volcanic deposits in the central northern Sierra Nevada. This is a composite drawn from measurements made at many different locations, as rarely are all units exposed at a single site. Unit thicknesses can vary between locations.

Cecil et al 2010

Cecil et al 2010

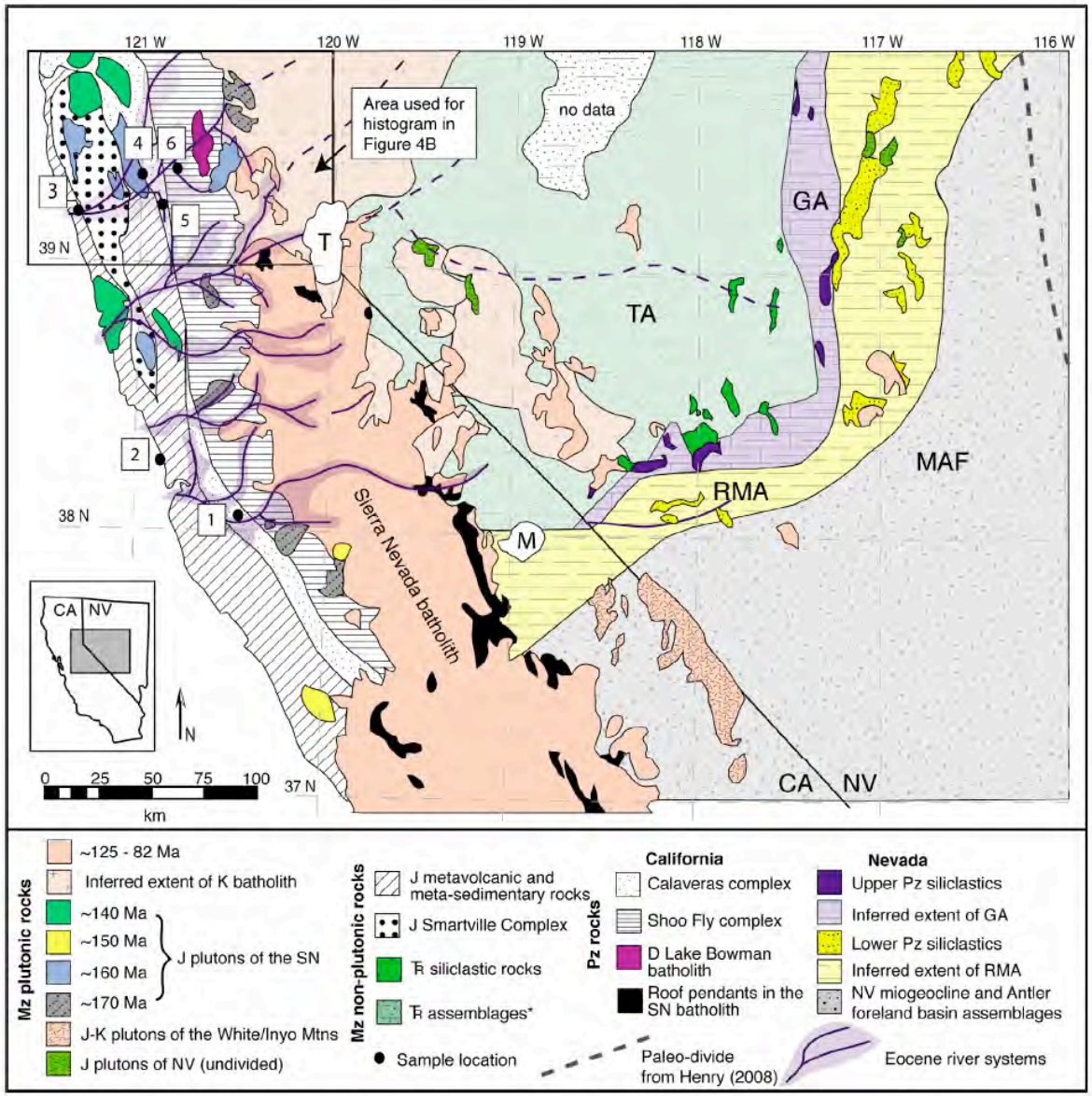

Figure 3. Generalized geologic map of the Sierra Nevada and central Nevada, modified after *Irwin and Wooden* [2001], *Gehrels and Miller* [2000], *Crafford* [2007], and *Van Buer et al.* [2009]. Pre-Eocene basement rocks in Nevada, where exposed, are shown in dark colors, and the inferred extent of basement terranes (compiled from *Gehrels and Miller* [2000], *Crafford* [2007], and *Van Buer et al.* [2009]) are shown in light colors. Sample locations are numbered and correspond to numbered age-probability plots in Figure 4a. Abbreviations are the same as for Figure 1b. Jurassic nonplutonic units make up the Foothills Belt (FB), and the Calaveras and Shoo Fly units make up the northern Sierra terrane (NST) shown in Figure 1b. T, Lake Tahoe; M, Mono Lake.

Cecil et al 2010

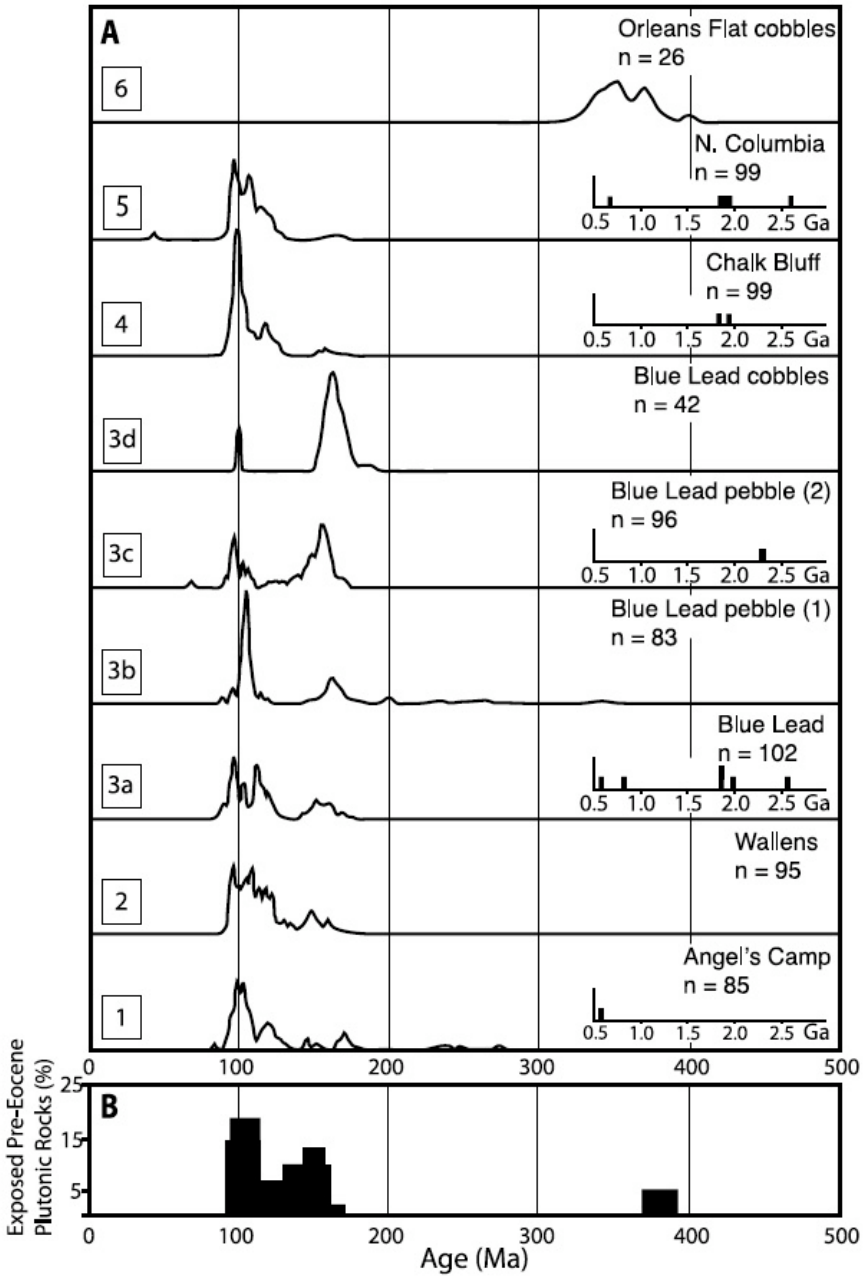

Figure 4. Detrital zircon age spectra for Eocene paleoriver deposits. (a) Data are plotted at two scales to emphasize the Mesozoic populations. Relative probability curves for Phanerozoic ages are plotted from 0 to 500 and inset are histograms of older grains plotted from 500 to 3000 Ma. (b) Relative age distribution of exposed pre-Eocene plutonic rocks in the northern Sierra Nevada (box in Figure 3).

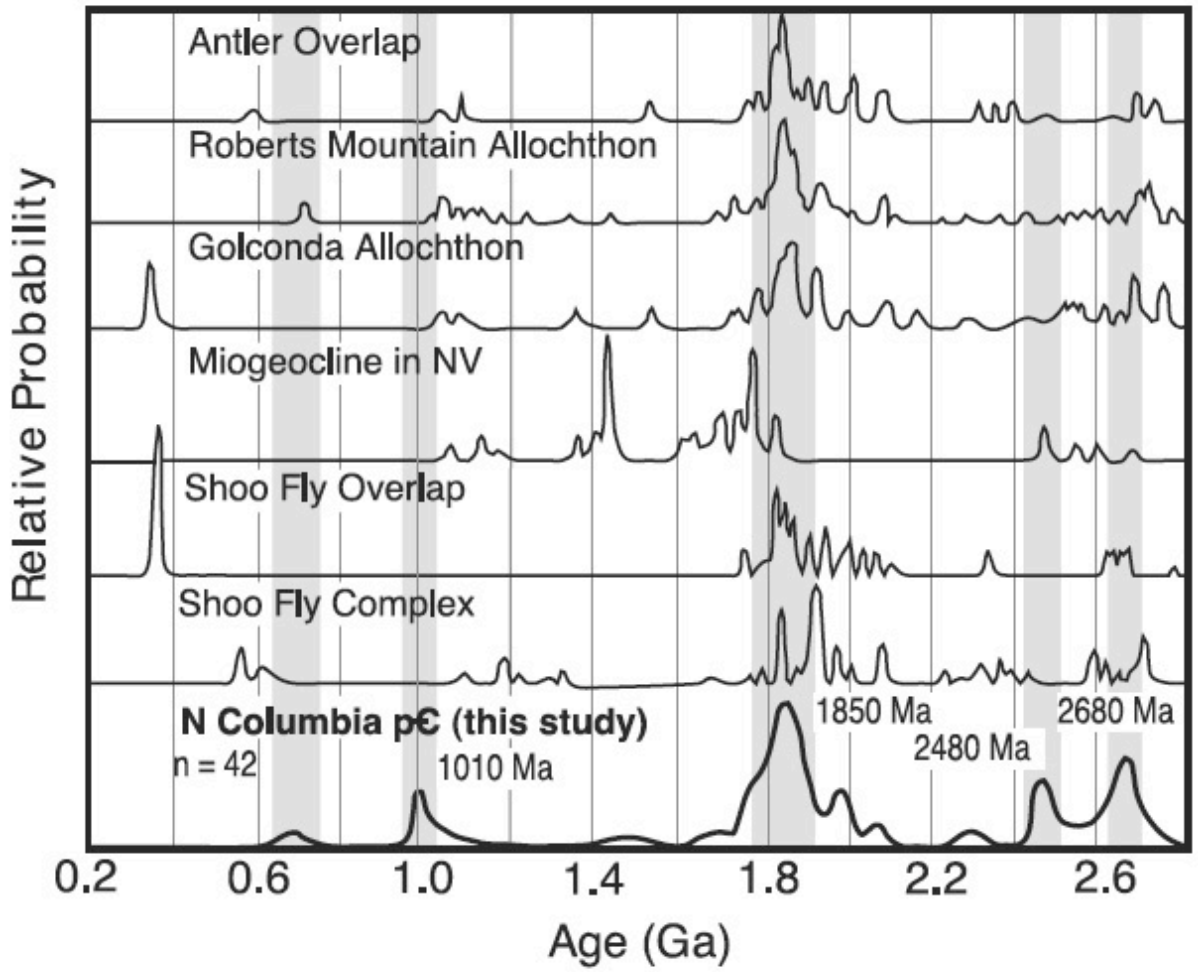

Figure 5. Comparison of pre-Mesozoic relative age-probability plots from basement terranes in the Sierra Nevada, Nevada, and from North Columbia Precambrian sample reported here (basement terranes are shown in Figure 1). Detrital zircon age distributions are from Antler Overlap [*Gehrels and Dickinson*, 2000], Roberts Mountain allochthon, [*Gehrels et al.*, 2000], Golconda allochthon, [*Riley et al.*, 2000], miogeocline in Nevada [*Gehrels et al.*, 1995], Shoo Fly Complex [*Harding et al.*, 2000], Shoo Fly overlap [*Spurlin et al.*, 2000].

Cecil et al 2010

Cecil et al 2010

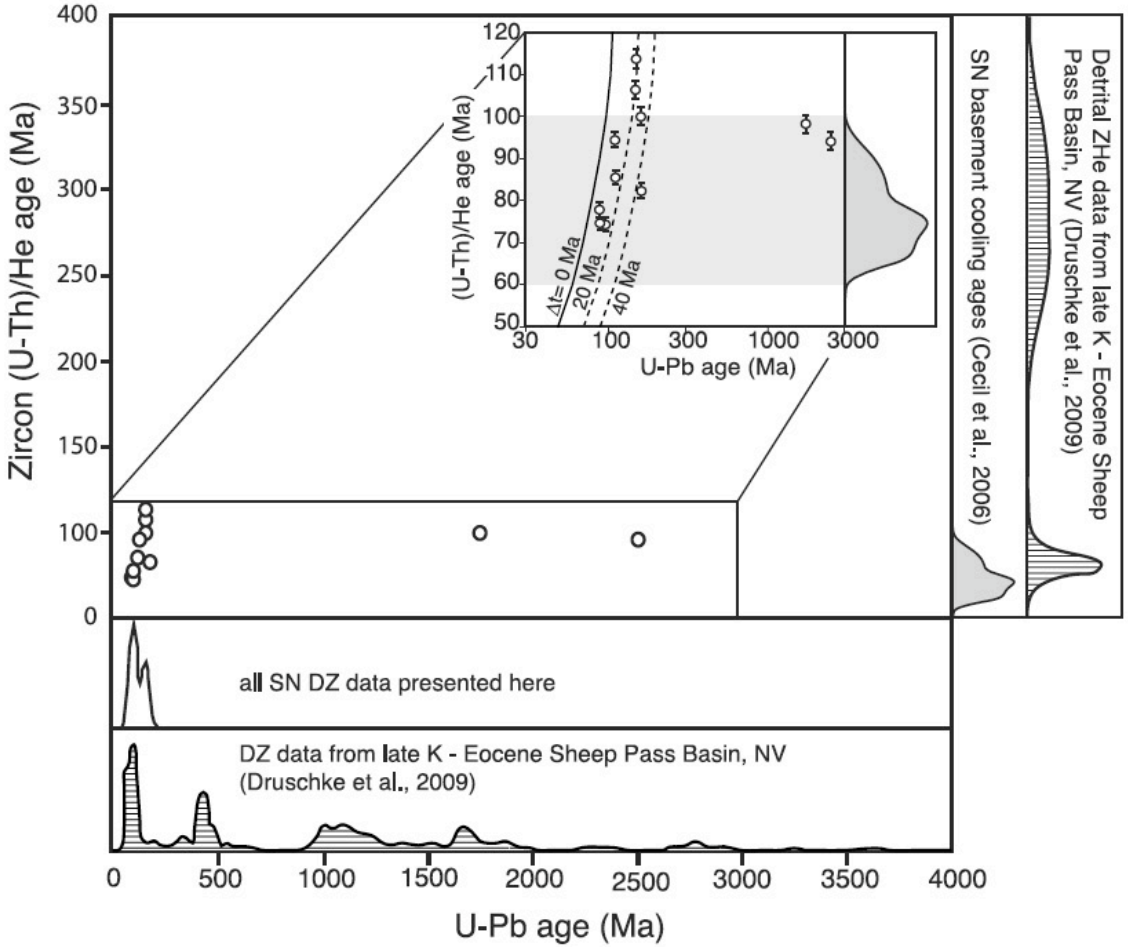

Figure 6. Detrital U-Pb and (U-Th)/He double dates of zircon grains from the Blue Lead sand sample (3a; Figure 2). (U-Th)/He ages are compared to (U-Th)/He zircon ages from Sierran bedrock samples (curve at right [from *Cecil et al.*, 2006]) and to detrital (U-Th)/He cooling ages of zircons from the late Cretaceous-Eocene Sheep Pass Basin, east central Nevada [from *Druschke et al.*, 2009]. U-Pb ages are compared to both the total distribution of detrital zircon ages measured here (Precambrian grains are of such low relative abundance that they do not plot visibly) and detrital zircon ages from the Sheep Pass Basin [*Druschke et al.*, 2009]. For clarity, our double-dated grains are shown again at different scale in the inset. U-Pb ages in the inset are plotted on a logarithmic scale. At such a scale, error bars are not visible. Zircon (U-Th)/He ages lie below, and are parallel to, the 1:1 He/Pb line (difference between crystallization and cooling age is zero; $\Delta t = 0$ Ma), as is expected for plutonic samples. Most grains fall within Δt contours drawn at 20 Ma and 40 Ma, indicating rapid cooling in the late Cretaceous, which is consistent with interpretations of bedrock cooling ages. Two multicycle grains (defined as those grains having $\Delta t > 300$ Ma [*Campbell et al.*, 2005]) have similar cooling ages, suggesting a common exhumation history. This is in contrast to similar ages detritus in Nevada, which has both Cretaceous and Permian cooling ages.

Cecil et al 2010

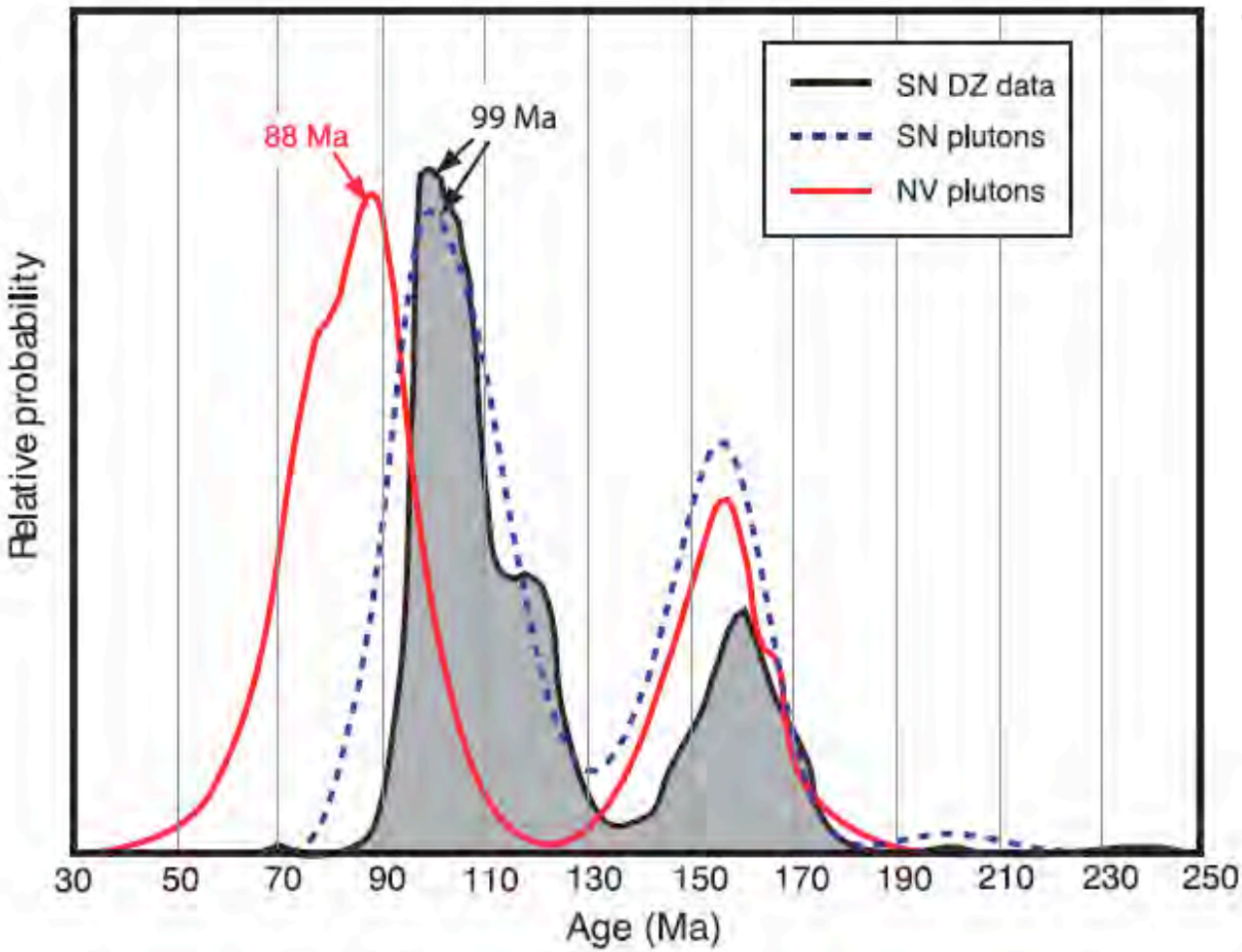

Figure 7. Relative probability curves for ages of Sierra Nevada plutons within area shown in Figure 2a and ages of Nevada plutons between 38°N and 41°N, both normalized to surface area. Pluton probability curves are compared to the relative probability plot of all Sierran detrital zircon data reported in this paper. Main Cretaceous peaks in the Sierra Nevada and Nevada are offset by 11 Myr. It should be noted that at present, Mesozoic plutons make up only 6% of the total Nevada surface area within the latitude bounds chosen, whereas >25% of the surface area of the northern Sierra Nevada today is composed of plutonic rocks. Exposed pluton area would presumably have been higher during the Eocene in both the Sierra Nevada and Nevada.

Cecil et al 2010

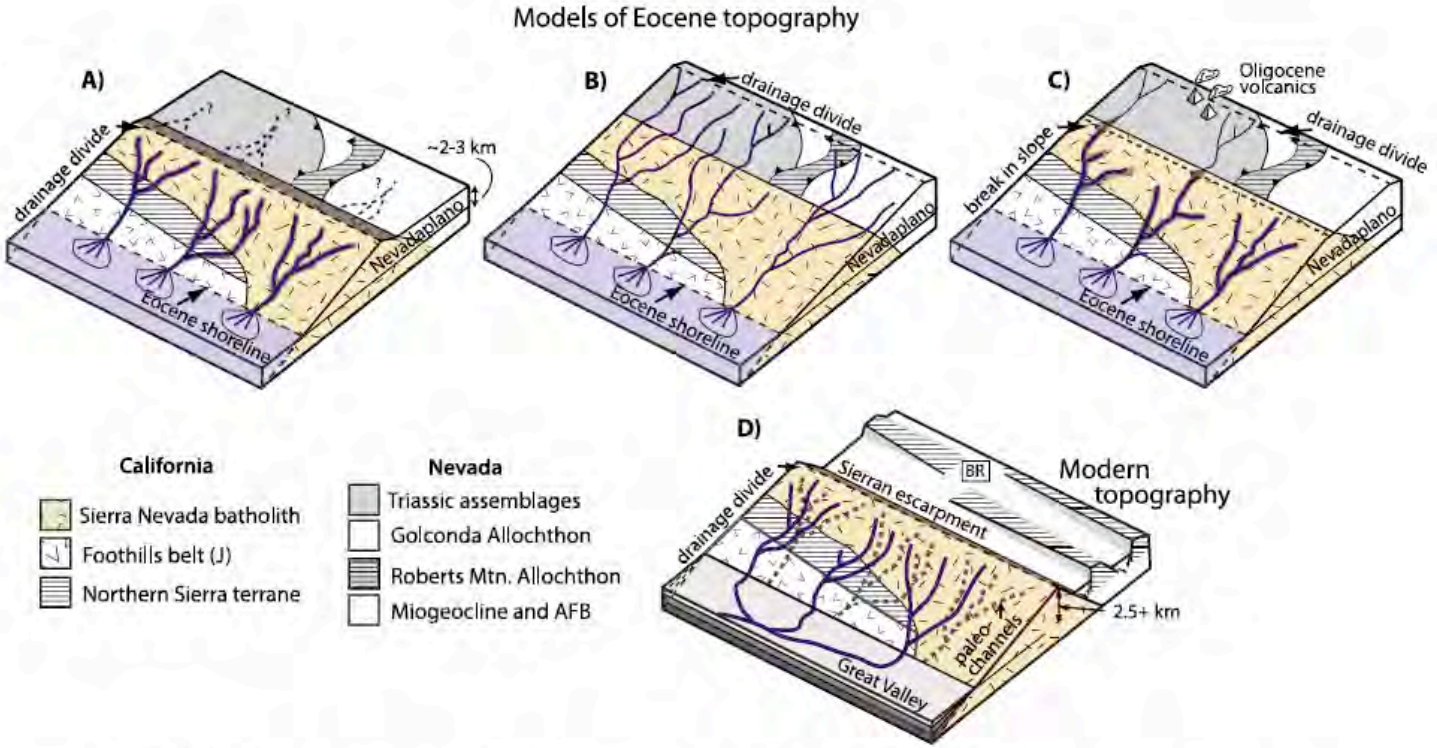

Figure 8. Schematic block models representing (a–c) Eocene and (d) modern topographic configurations of the Sierra Nevada and adjacent Nevada highlands (Eocene)/Basin and Range (modern). Figure 8a shows paleotopography of the Sierra Nevada best supported by the detrital zircon data presented herein. A drainage divide, in roughly the same position as that of the modern one, separates the Sierra from the interior Nevadaplano. Paleorivers are relatively steep, with small catchments, sourced entirely within the Sierra Nevada block. Crestal elevations are assumed to be at least 1.5 km, based on paleoelevation estimates for the Nevadaplano. The western flank of the Sierra slopes westward at a gradient similar to the modern one. Figure 8b shows traditional model of Sierra Nevada paleotopography based on a regionally developed erosion surface and the meandering and alluviated nature of Eocene rivers. This model implies a shallow gradient for the western Sierran flank, with relatively low-slope rivers draining a large area, and is a poor fit to the detrital zircon data presented here. In Figure 8c paleorivers drain westward across the Nevadaplano in nonerosive channels but must incise and exclusively incorporate Sierran detritus to the west to be consistent with our provenance data. This model requires a change in slope or some other mechanism for changing erosive power of the paleorivers at or near the modern divide but has the benefit of not requiring a large (>150 km) eastward shift in drainage divide position before deposition of Oligocene ash flows in Sierran paleorivers. In Figure 8d the period from ~5 Ma to the present is marked by the extensional collapse of the nearby Nevada highlands and the development of the Sierran frontal escarpment, perhaps accompanied by moderate uplift of the range crest. Paleochannels (gray dashed) are abandoned, and modern drainages (dark blue) are incised. BR, Basin and Range.

Whiskey Lake, McKinley County, New Mexico

Cather et al 2010

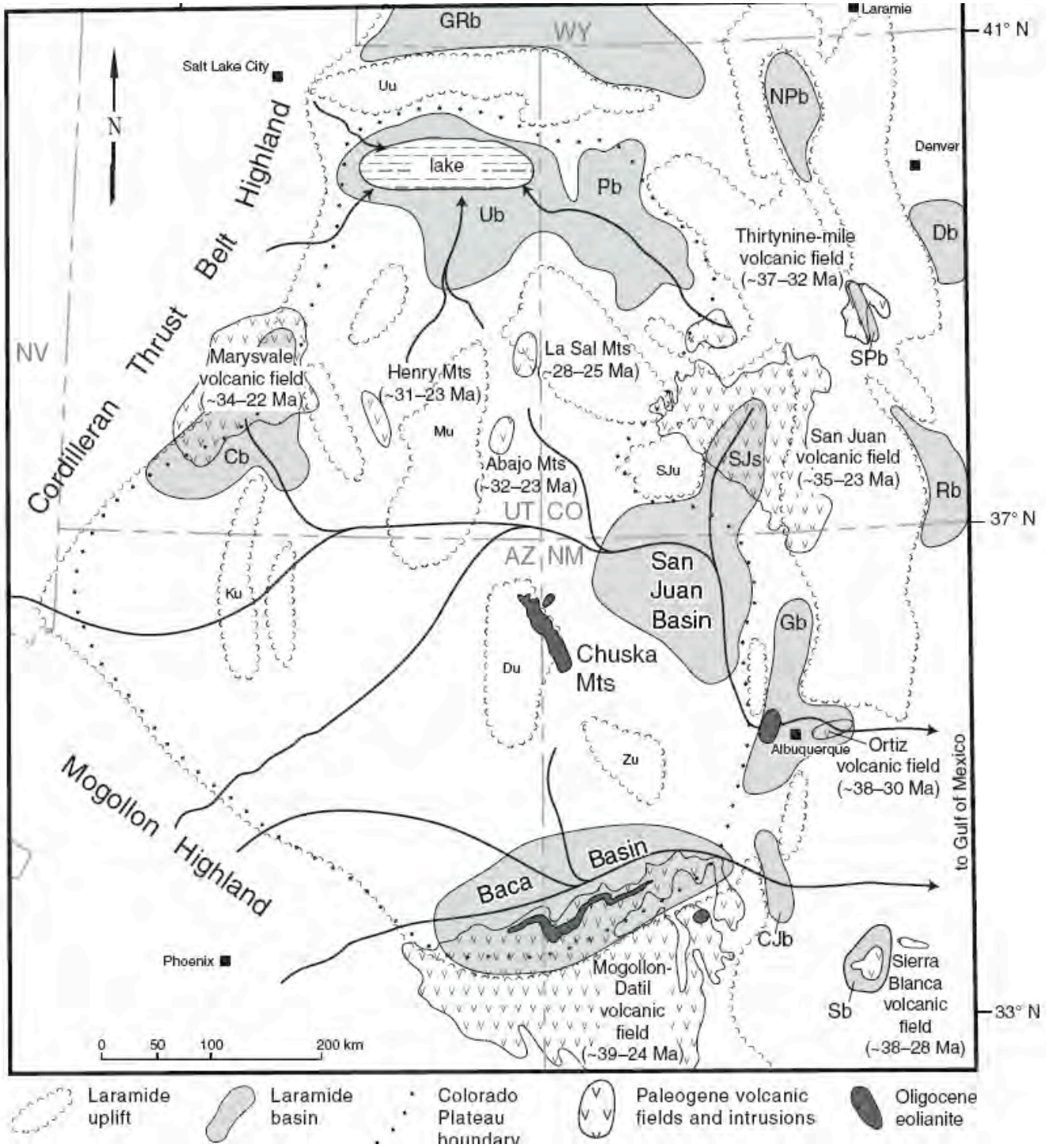

Cather et al 2010

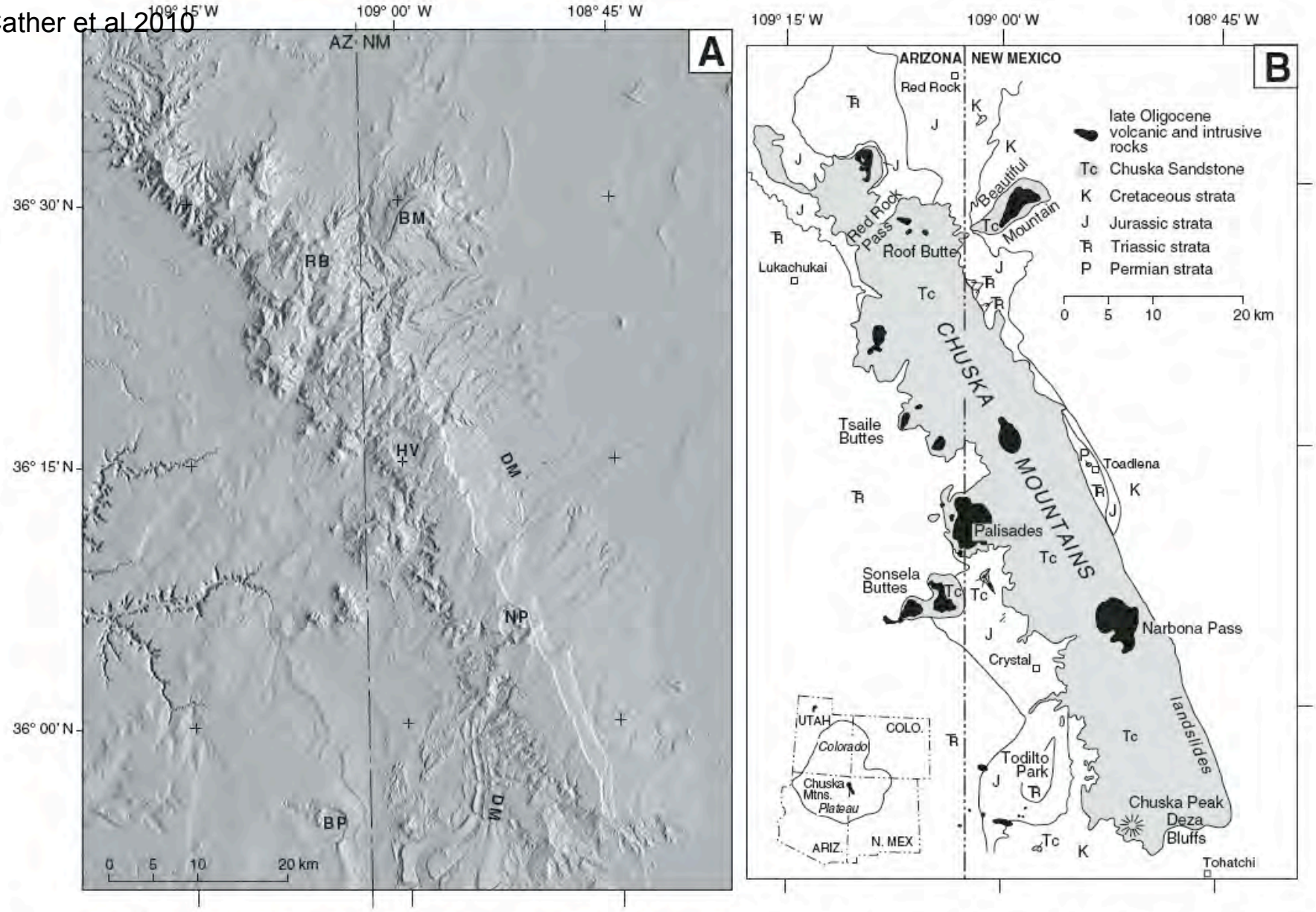

Figure 2. (A) Digital elevation model for the Chuska Mountains area. Flat top of the southern Chuska Mountains is defined by silica-cemented zones within the Chuska Sandstone that formed during early, phreatic diagenesis (see text). Note the eastern boundary structure of the Laramide Defiance uplift (the Defiance monocline, DM) is buried by the Chuska Sandstone. Selected features of the Navajo volcanic field are Buell Park diatreme (BP), Narbona Pass maar (NP), sill at Beautiful Mountain (BM), and the Hidden Valley maar (HV). Volcanic necks at Roof Butte (RB) mark highest part of range (2980 m). (B) Simplified geologic map of the Chuska Mountains area, after Wright (1956).

Cather et al 2010

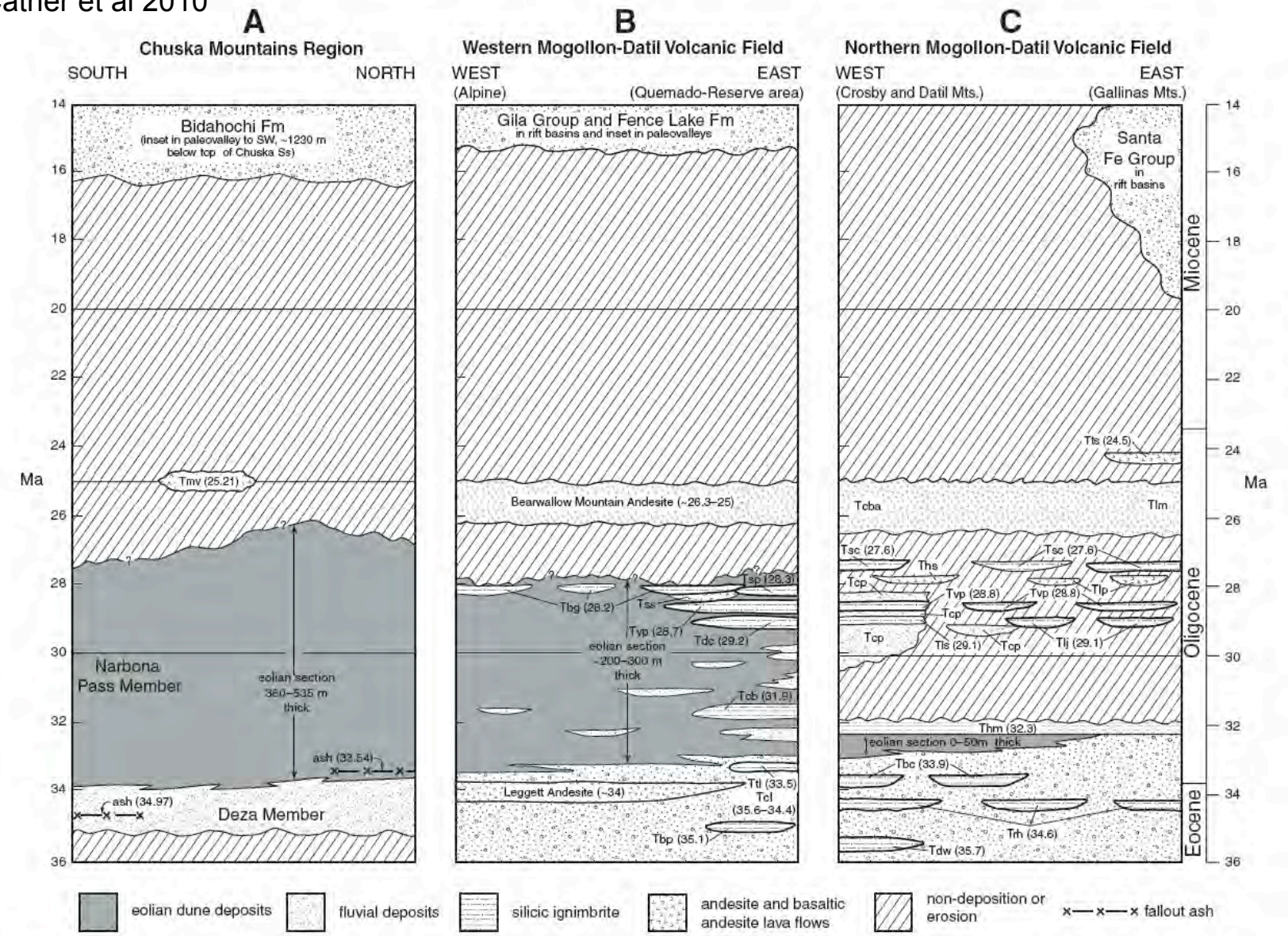

Figure 5. Chronostratigraphic correlation diagram for eolianites and associated rocks in the Chuska Mountains and the Mogollon-Datil volcanic field. (A) Chuska Mountains, showing members of Chuska Sandstone. (B) Western Mogollon-Datil field. (C) Northern Mogollon-Datil field. See text for sources of radioisotopic age data. Tmv—lava flows associated with maar at Narbona Pass; Tbp—Bishop Peak Tuff; Tcl—volcaniclastic unit of Cañon del Leon; Ttl—tuff of Luna; Tcb—Caballo Blanco Tuff; Tdc—Davis Canyon Tuff; Tvp—Vicks Peak Tuff; Tss—Squirrel Springs Canyon Andesite; Tsp—Shelly Peak Tuff; Tbg—Bloodgood Canyon Tuff; Tdw—Datil Well Tuff; Trh—Rock House Canyon Tuff; Tbc—Blue Canyon Tuff; Thm—Hells Mesa Tuff; Tcp—South Crosby Peak Formation; Tlj—La Jencia Tuff; Tlp—La Jara Peak Basaltic Andesite; Ths—basaltic andesite of Hidden Spring; Tsc—South Canyon Tuff; Tlm—Lion Mountain Andesite; Tcba—basaltic andesite of Crosby Mountains; Tts—tuff of Turkey Springs. Numbers in parentheses indicate radioisotopic age (Ma).

Cather et al 2010

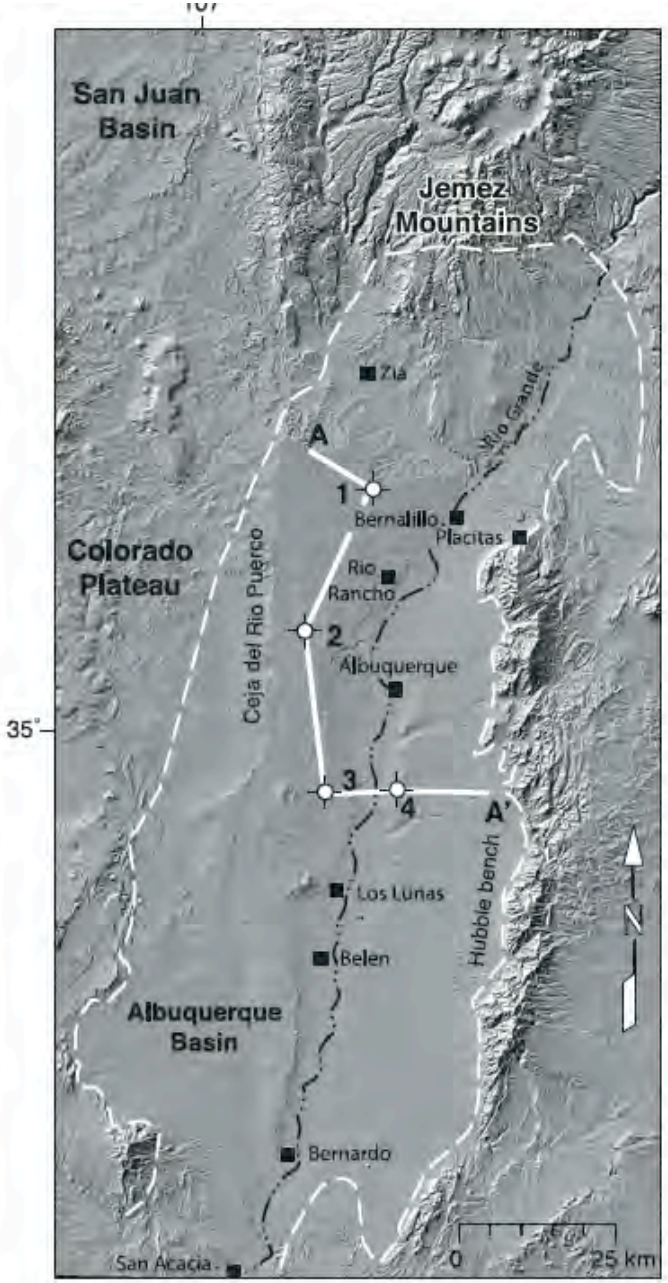

Figure 8. Digital elevation model for the Albuquerque Basin area, showing basin boundaries (dashed lines) and cross-section line (Fig. 10). Wells are: (1) Tamara #1-Y; (2) West Mesa Federal #1; (3) Shell Isleta #2; (4) TransOcean Isleta #1.

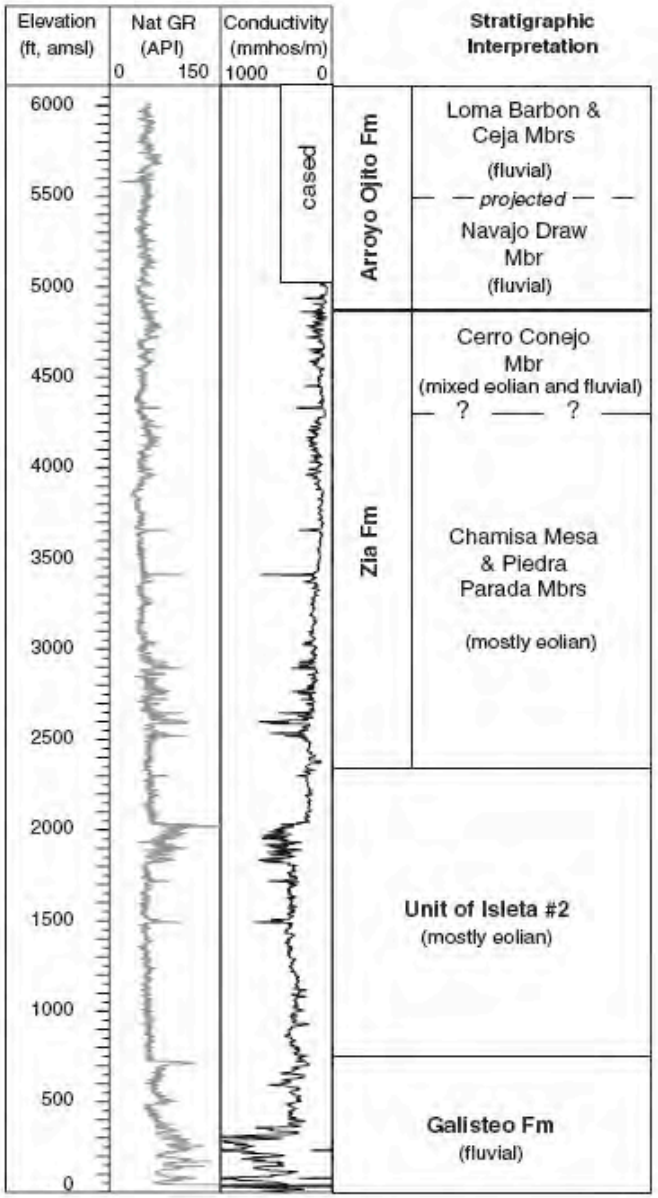

Figure 9. Gamma-ray and conductivity logs for Tamara #1-Y well. The unit of Isleta #2 is interpreted to be largely eolian in this well. amsl—above mean sea level; mmhos—millimhos (= 10^{-3} siemens).

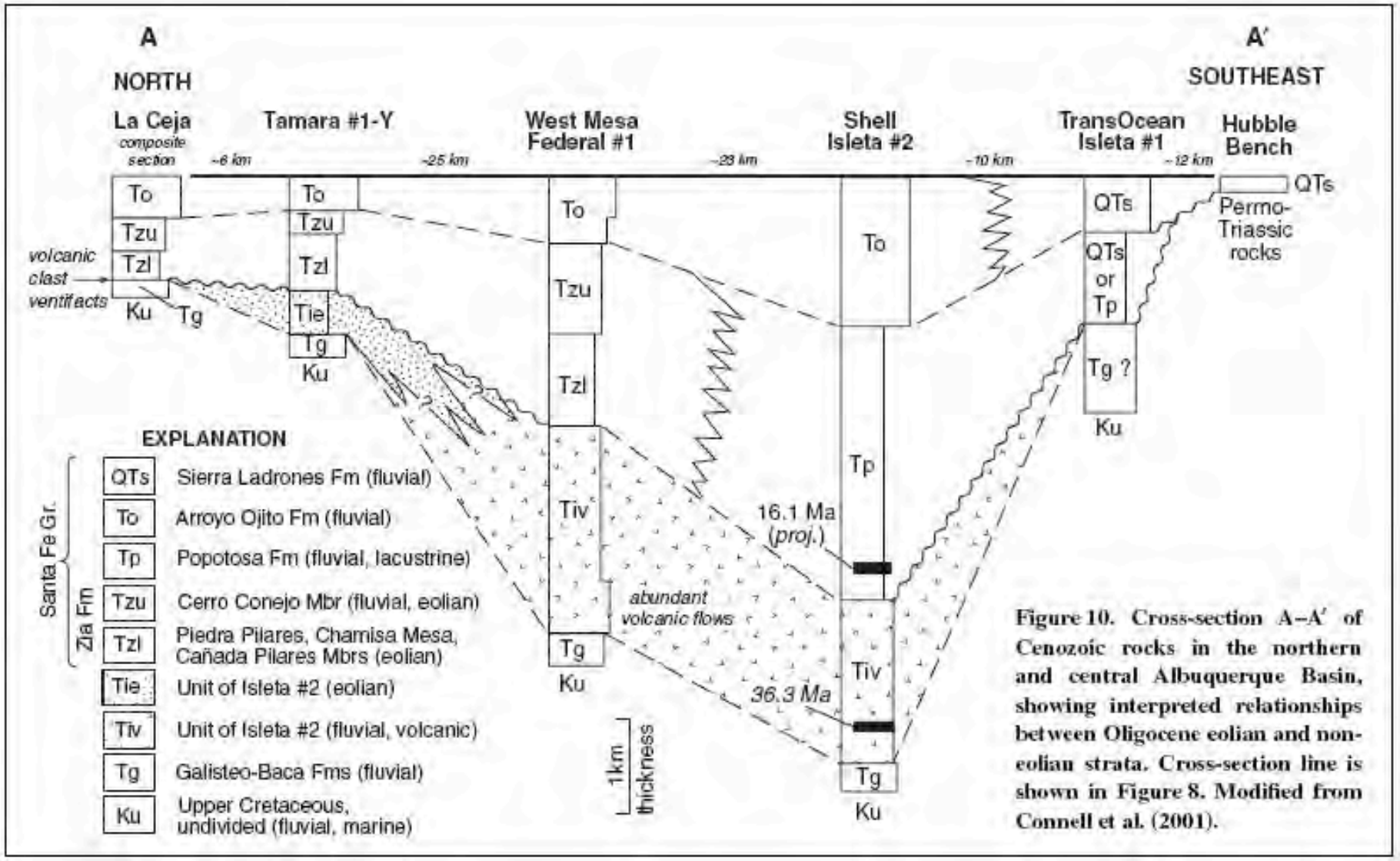

Figure 10. Cross-section A–A′ of Cenozoic rocks in the northern and central Albuquerque Basin, showing interpreted relationships between Oligocene eolian and non-eolian strata. Cross-section line is shown in Figure 8. Modified from Connell et al. (2001).

Cather et al 2010

Cather et al 2010

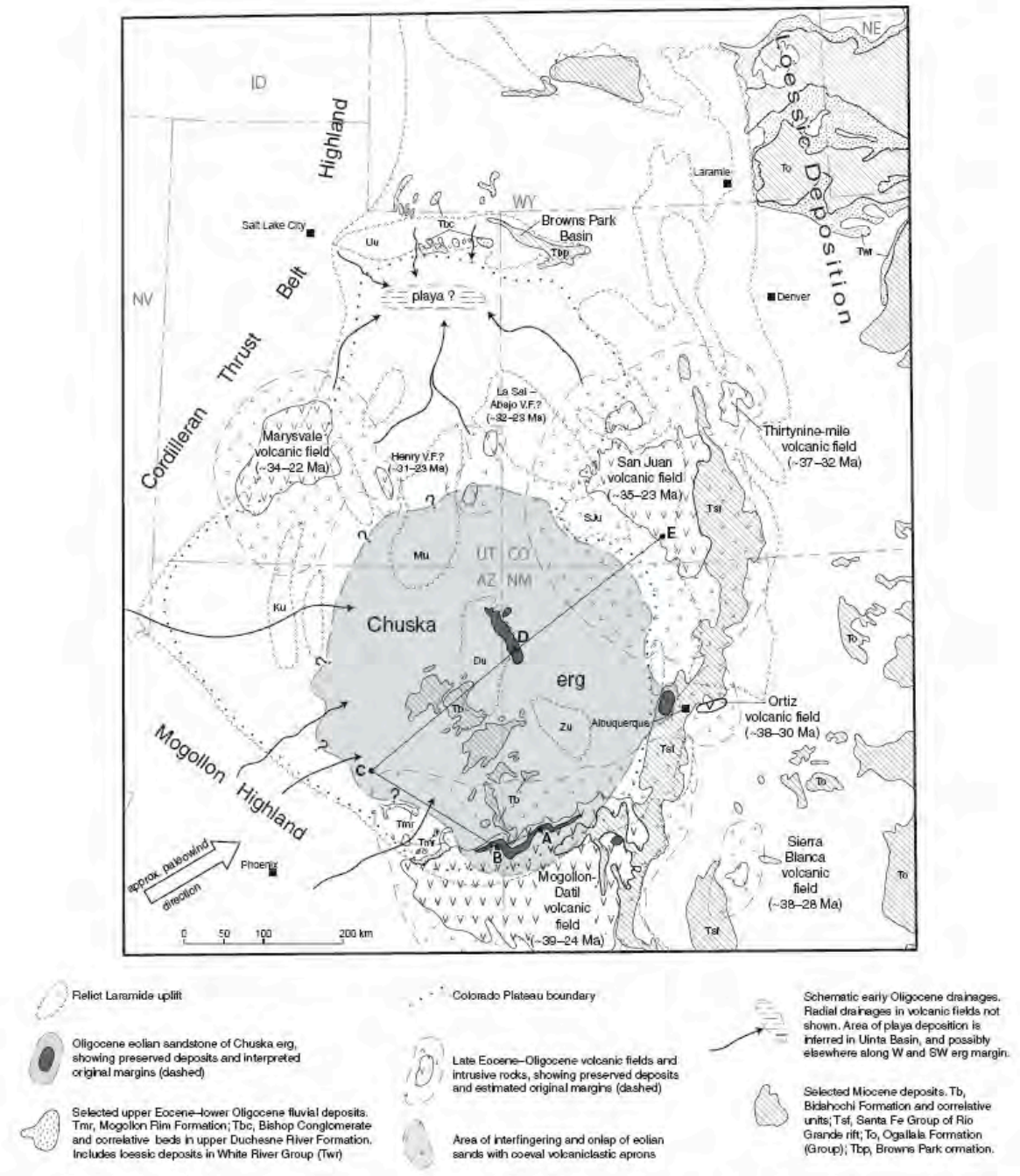

Figure 13. Map showing interpreted early Oligocene paleogeography in the Colorado Plateau-Rocky Mountain area in relation to relict Laramide uplifts and selected Miocene sedimentary deposits. A–E is line of section for Figure 14. Selected Laramide uplifts are: Du—Defiance uplift; Zu—Zuni uplift; Ku, Kaibab uplift; Mu—Monument uplift; SJu—San Juan uplift; Uu—Uinta uplift. See text for discussion.

Cather et al 2010

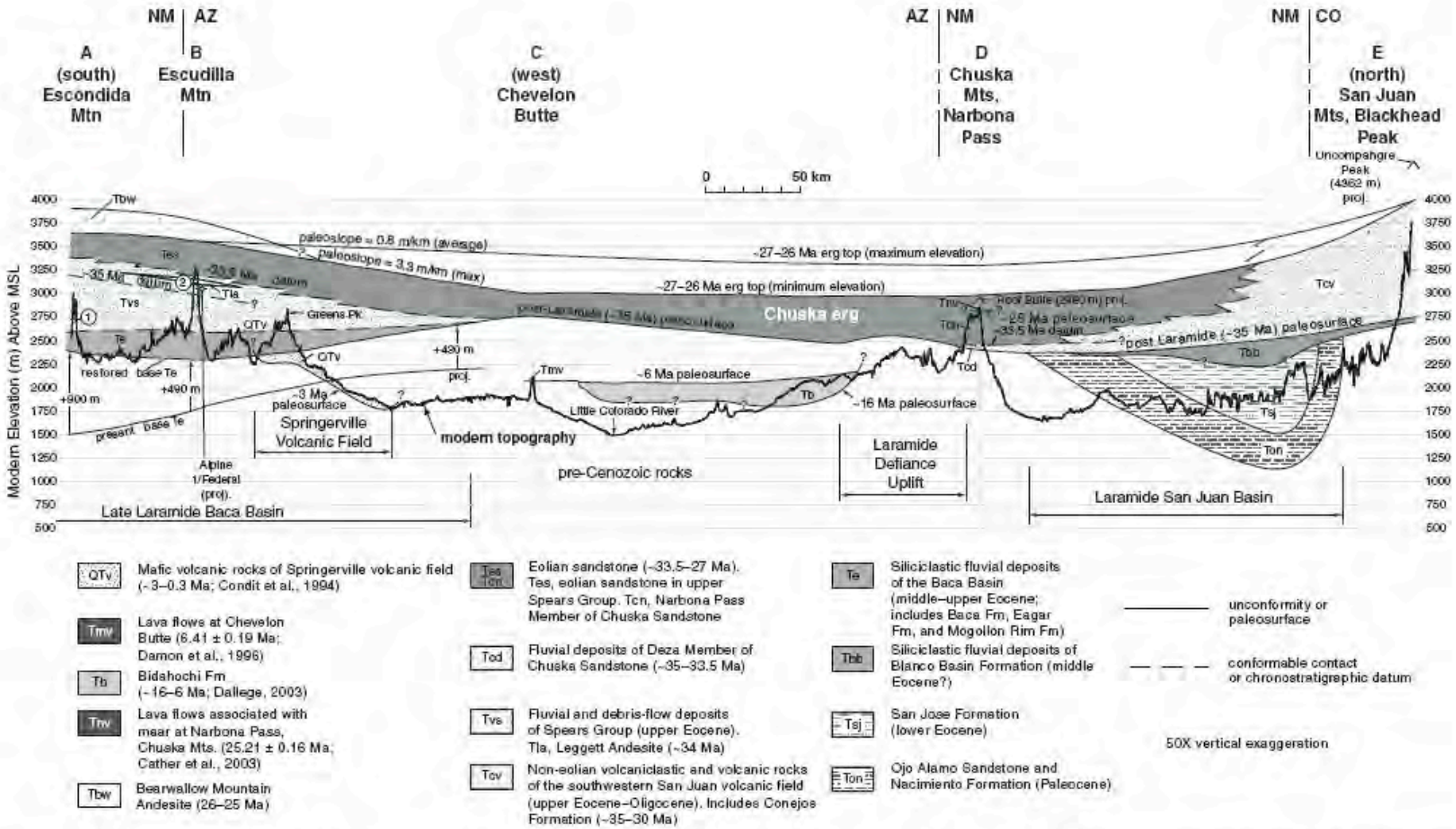

Figure 14. Regional cross-section showing present-day elevations of reconstructed stratigraphic successions of Paleocene to Pleistocene age in relation to modern Colorado Plateau topography. Note that the elevation of strata in the southern (left) part of the cross section has been restored (vertical arrows above present base of Te) to account for structural lowering of the southern Colorado Plateau margin (see text). Unrestored elevations of top of eolian succession at (1) Escondida Mountain and (2) Escudilla Mountain shown by tic marks and circled numerals. Approximate ~35 Ma chronostratigraphic datum, given by base of volcaniclastic unit of Cañon del Leon (35.6 Ma; Chamberlin and Harris, 1994) at Escondida Mountain and by the Bishop Peak Tuff (35.1 Ma, projected from nearby Alpine1/Federal well) at Escudilla Mountain; A range of elevations for the reconstructed ~27- to 26-Ma top surface of the Chuska erg is depicted, using end-members based on steep versus average slopes of modern ergs (see text). The topographically highest points in the Chuska Mountains and San Juan Mountains are projected from areas north of the line of section.

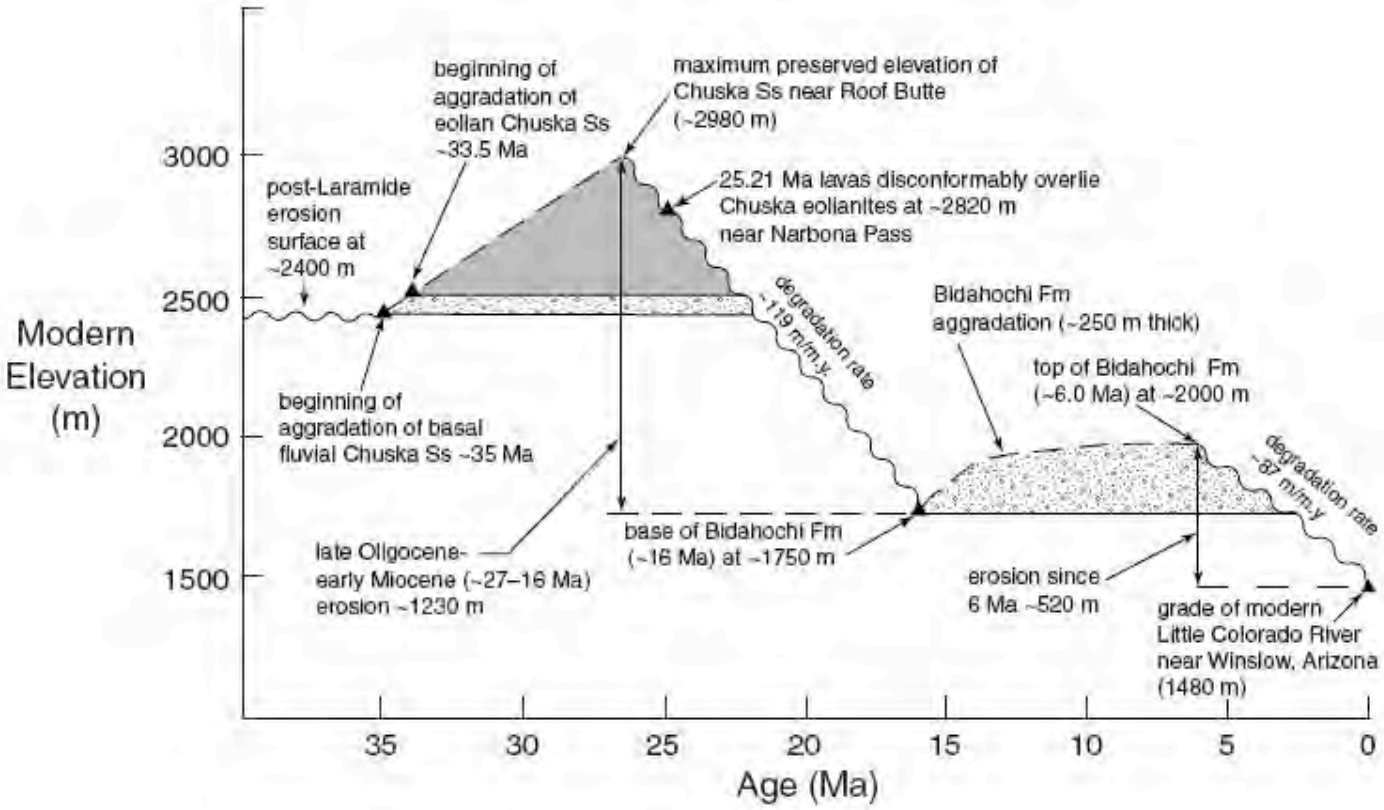

Figure 15. Late Eocene to Recent aggradation and exhumation history of the central and southern Colorado Plateau relative to present-day elevations, based on a conservative (minimum) estimate of elevation of Chuska erg surface. Note that the Chuska Sandstone and Bidahochi Formation outcrops are ~100 km apart.

Cather et al 2010

Upper Cretaceous near Bardwell, Texas

Upper Cretaceous Beds “Post Office Outcrop” Dallas, TX

Upper Cretaceous Tropic Shale, nr Escalante, UT

Upper Cretaceous, I-70

Upper Cretaceous Capitol Reef N P

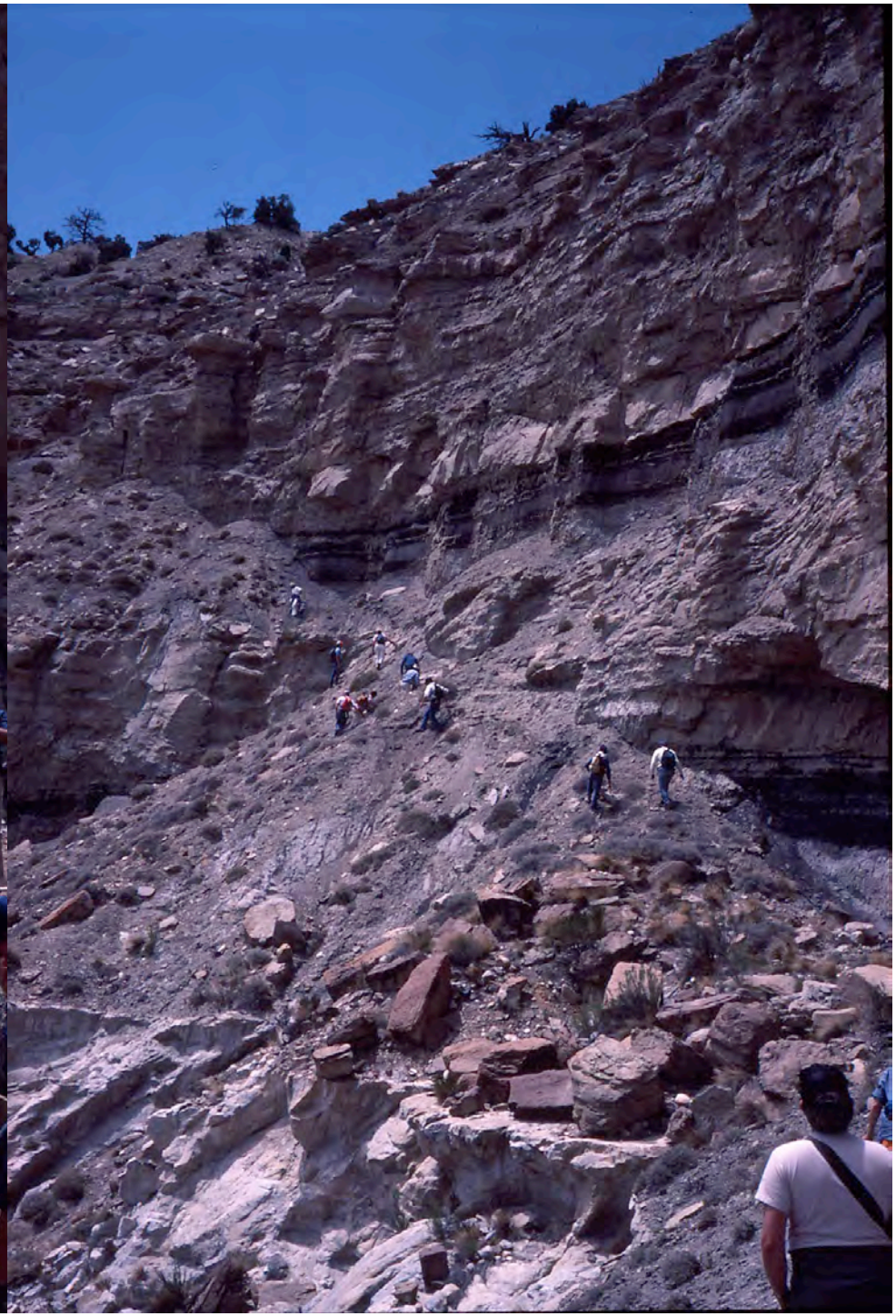

Book Cliffs from I-70 Green River, Utah

Mancos Shale

Upper Cretaceous, near Woodside, Utah

Upper Cretaceous near Cortez, Colorado

Upper Cretaceous Shelf Sandstones

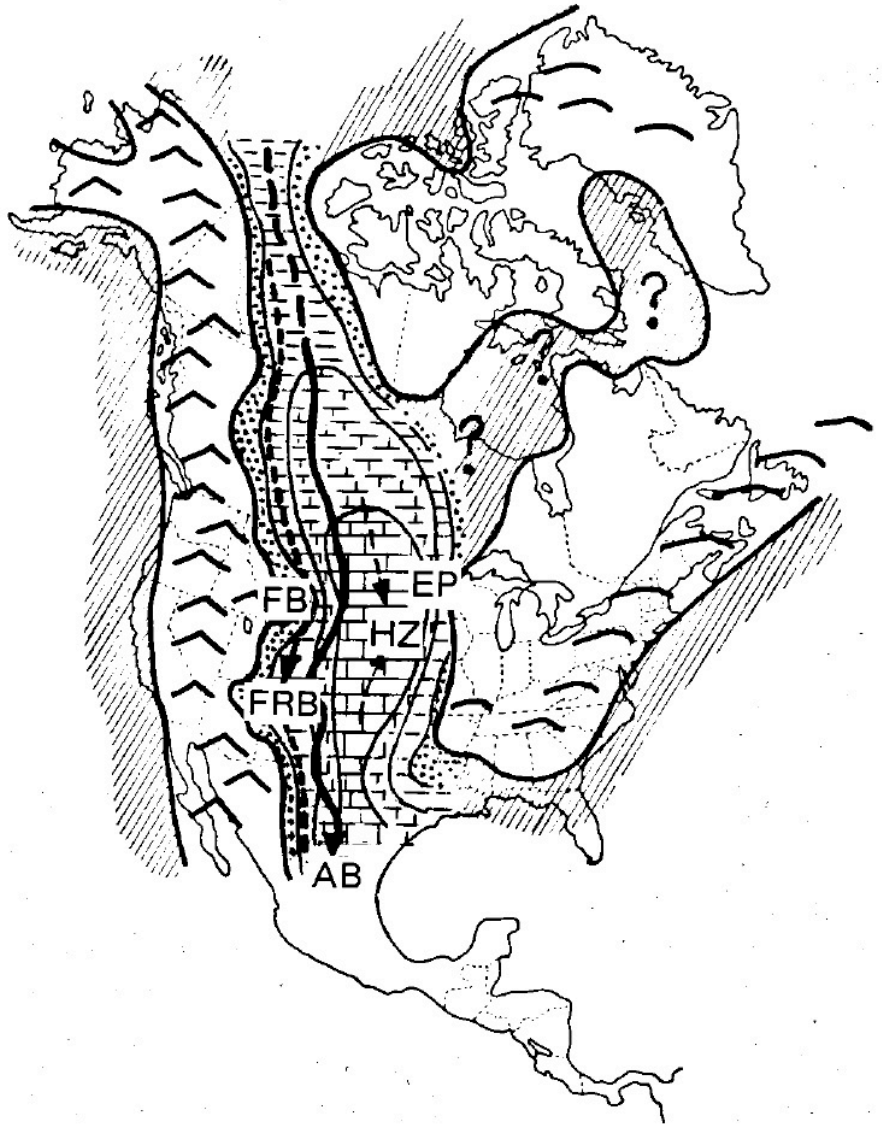

Figure 1. Extent of the Western Interior Cretaceous Seaway, and major facies distribution patterns, within each of the four major tectonic zones of the basin during peak Lower Turonian eustatic rise and transgression. Modified from Kauffman (1969), and Williams and Stelck (1975, Fig. 5). Key: *AB*-Axial Basin; *EP*-Eastern Stable Platform; *FB*-Foreland Basin; *FRB*-Forebulge zone; *HZ*-Hinge Zone.

Kauffman 1984

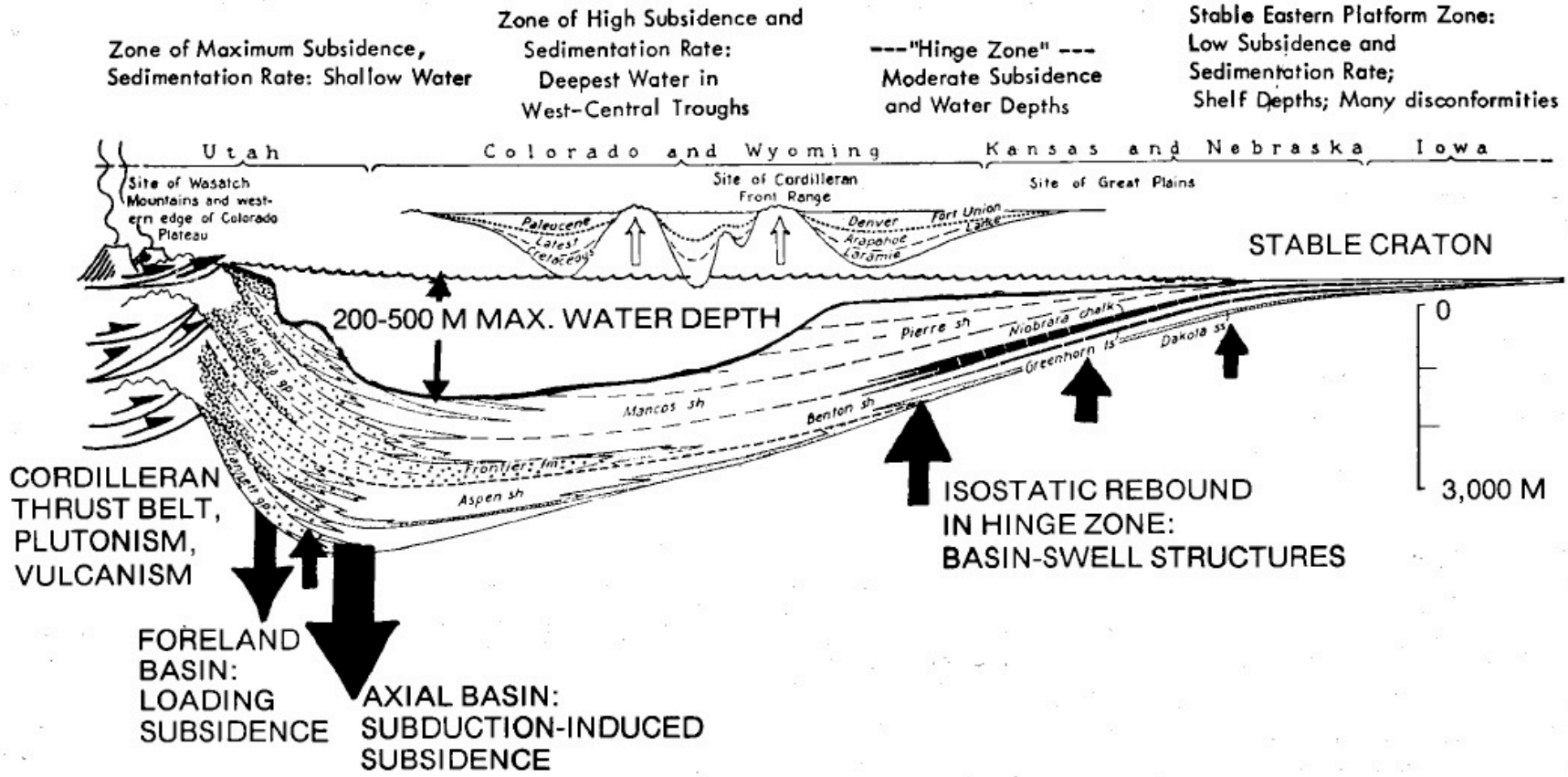

Figure 2. Generalized structural and stratigraphic cross-section through the Western Interior Cretaceous Basin (modified from Kauffman, 1977a), modeled after a peak transgressive phase and eustatic high-stand, showing the major structural divisions of the basin, sediment thicknesses and facies characteristic of each division, and relative paleobathymetry. Position, direction, and size of arrows indicate relative thrusting, subsidence, and uplift at the western margin and within the basin during periods of eustatic rise.

Kauffman 1984

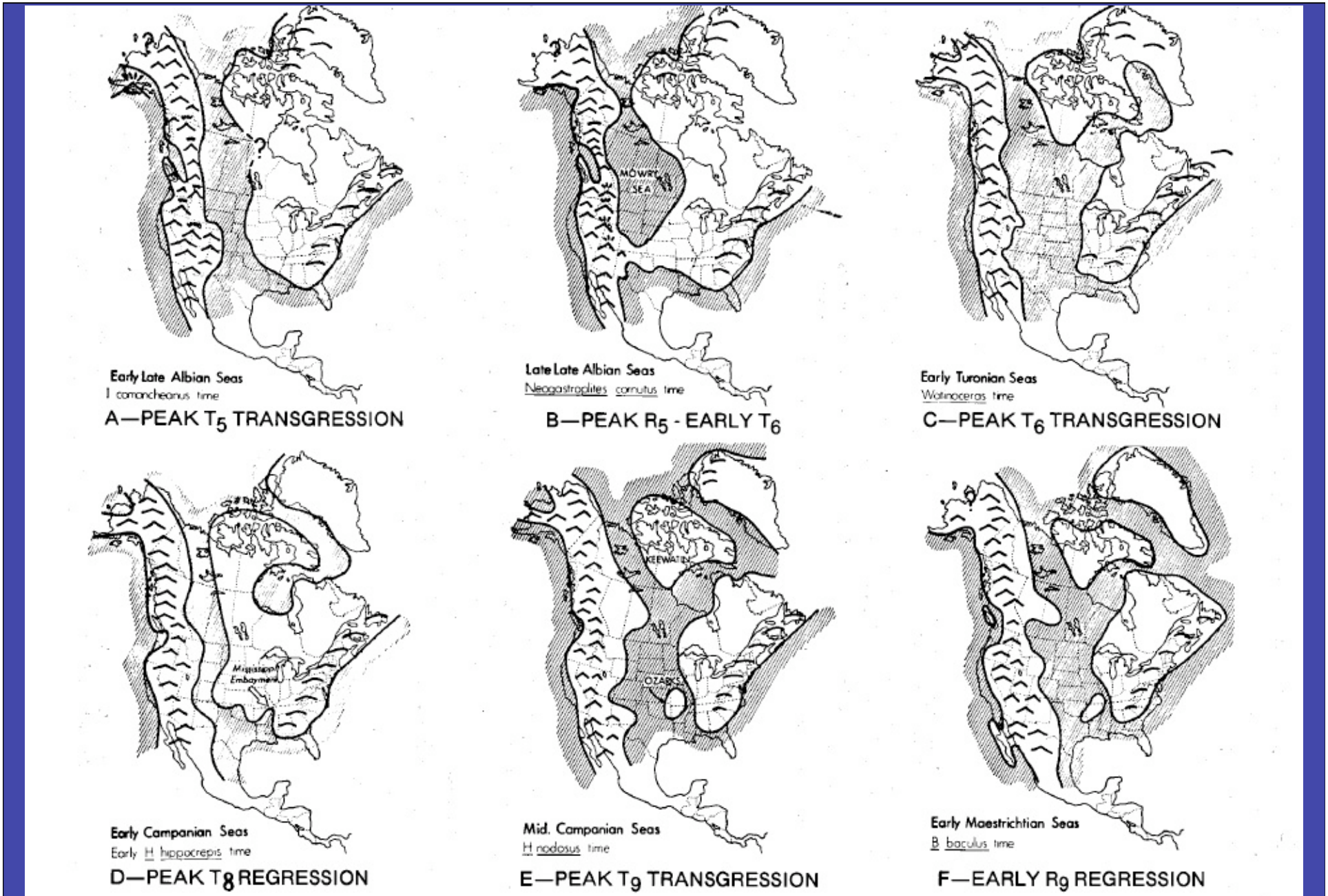

Figure 3. Generalized maps of North America showing extent of Western Interior Cretaceous Seaway during major third-order eustatic fluctuations (transgressions and regressions, utilizing Kauffman's 1977a nomenclature), in temporal progression from A – F (oldest to youngest). Maps from Williams and Stelck, 1975, slightly modified.

Kauffman 1984

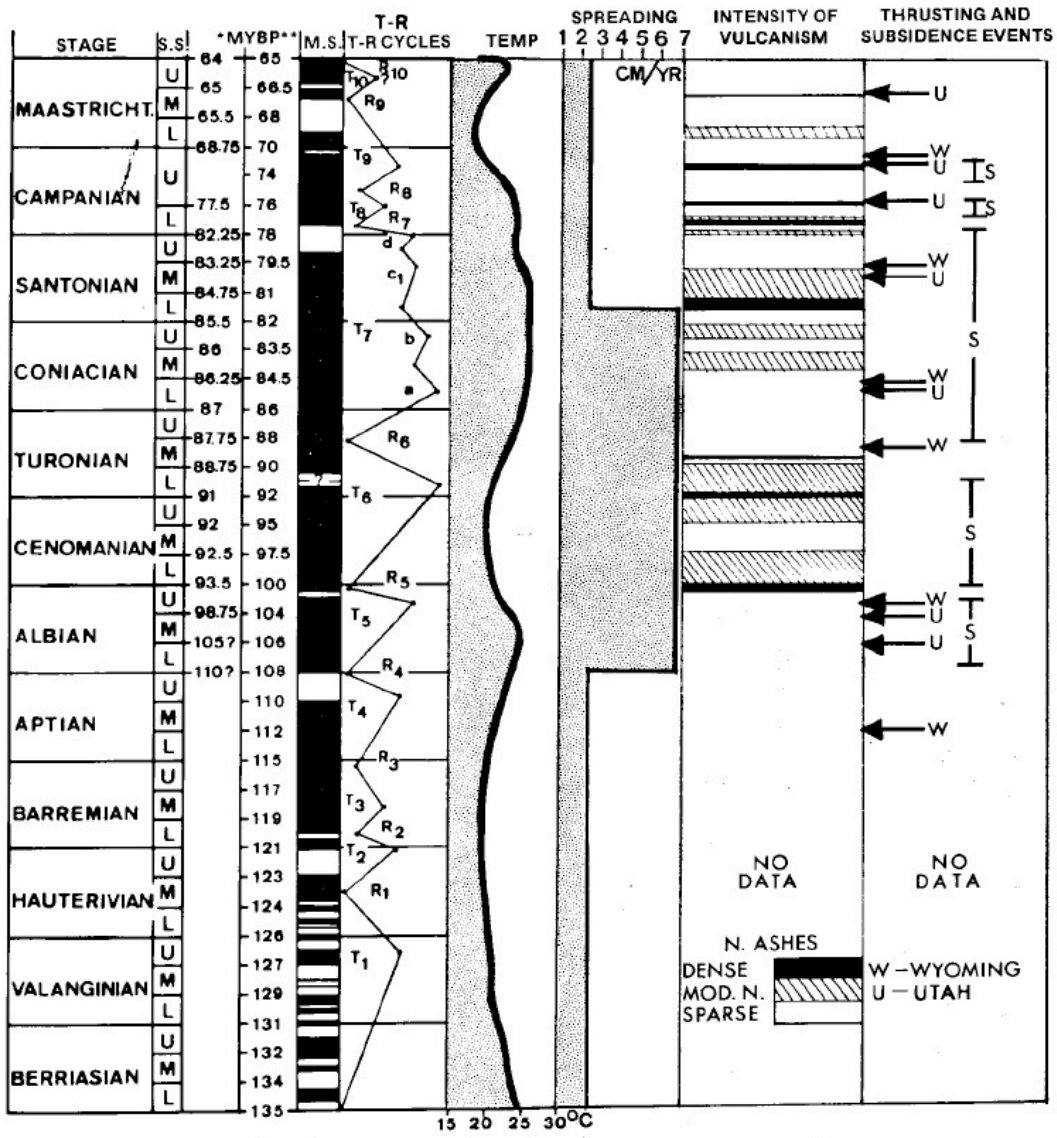

Figure 4. Geochronologic and magnetostratigraphic dating of global sealevel changes; third-order transgressive-regressive (T-R) epicontinental cycles (from Kauffman, 1977a); average marine temperature fluctuations (averaged from data in Kauffman, 1977a); Atlantic and Pacific half-spreading rates averaged (Larson and Pitman, 1972; Sheridan *et al.*, 1982); episodes of intense (black) and moderately intense (striped) volcanism, measured by number and magnitude of volcanic ash events (partially from Kauffman *et al.*, 1976); initiation of major thrusting (arrows) in Utah (U) and Wyoming (W) (data from Villien and Kligfield, pers. commun., 1984, and Wiltschko and Dorr, 1983, respectively); and times of most active basin subsidence (S), determined stratigraphically, in the Western Interior Seaway. Note correlation of active tectonism, subsidence, and volcanism with periods of active plate spreading and global sealevel rise, as contrasted to periods of relative tectonic quiescence during sealevel fall. Generalized time scales from Kauffman (Western Interior Seaway, left column, 1977a) and Van Hinte (global; right column, 1976).

Kauffman 1984

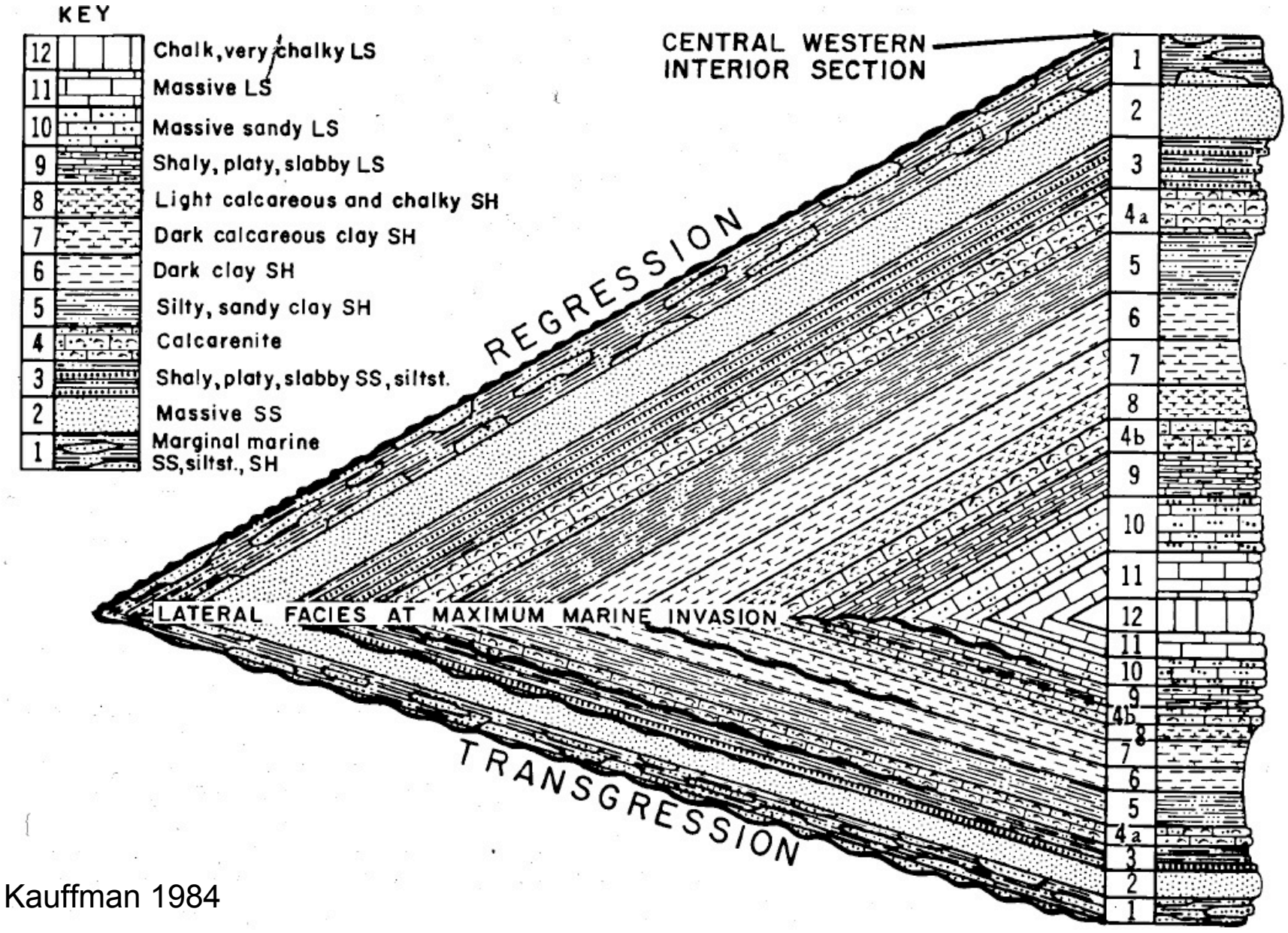

Kauffman 1984

Figure 5. Generalized model of a symmetrical Cretaceous cyclothem, reflecting deposition during a third-order tectonoeustatic fluctuation, in the center (right) and shallow marginal platform (left) of a hypothetical epicontinental sea (based on center to eastern margin transect of Western Interior Cretaceous Basin). Modified after Kauffman (1969, 1977a) in which the upward-fining transgressive facies (1-12) and upward-coarsening regressive facies (12-1), are defined in detail as preserved in the axial part of the Western Interior Basin. Note shoreward-basinward diachronism of facies during transgression-regression, bounding disconformities, and concentration of intra-cycle disconformities on transgressive hemicycle.

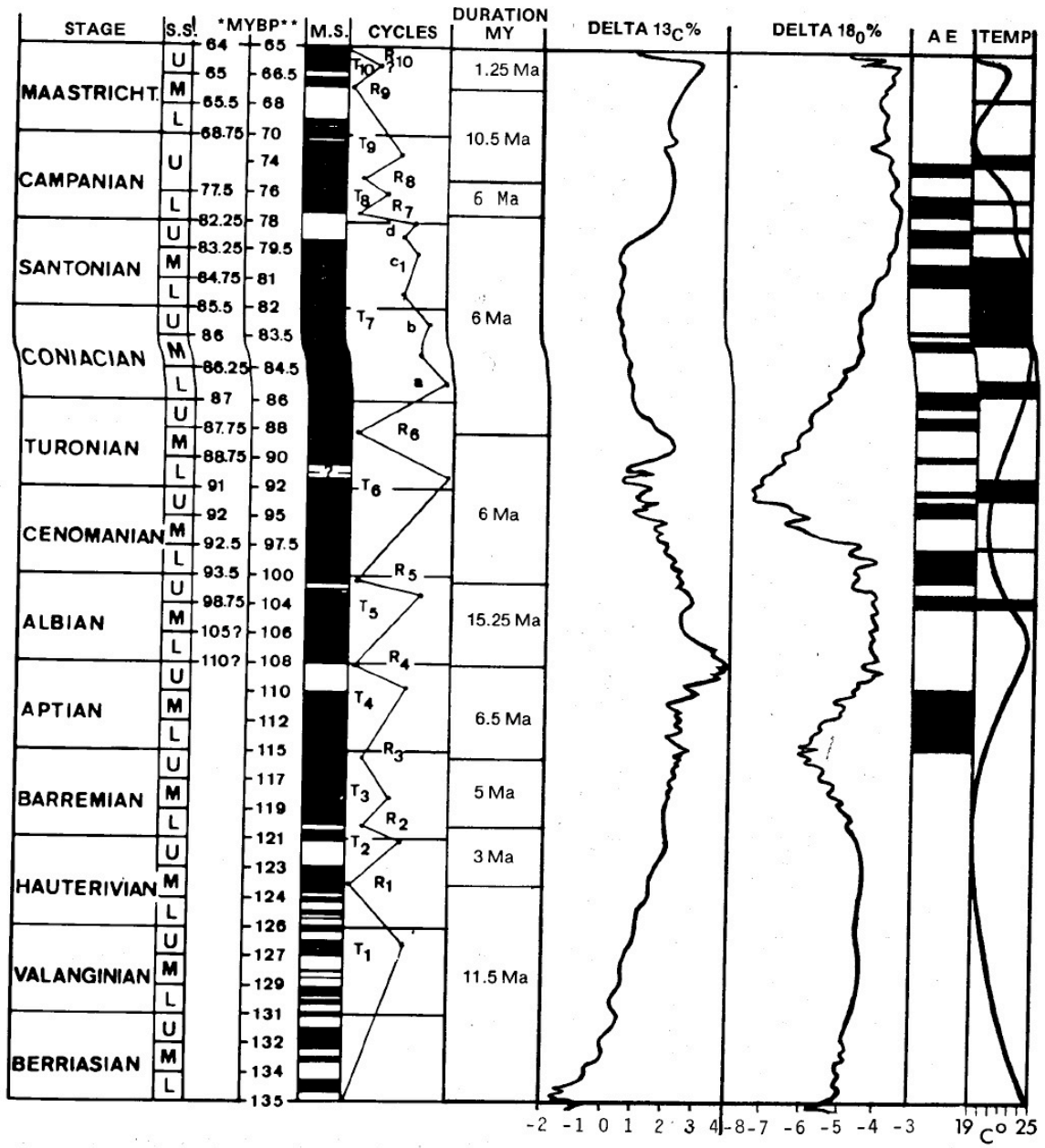

Figure 6. Global third-order tectonoeustatic cycles (T_1-R_1) plotted against magnetostratigraphic and radiometric standards (from Kauffman, 1977a; see explanation, Fig. 4 herein). T_5-T_{10} widely inundated the Western Interior Cretaceous Basin. Note radiometric times of peak transgressive and regressive events, cycle durations, and major paleoceanographic fluctuations as defined by geochemical profiles ($\delta^{13}C_{arb}$, $\delta^{18}O_{org}$). Geochemistry generalized from Scholle and Arthur (1980); Pratt (1983). Right hand columns show anoxic events (AE) and rapid warm-water incursions (TEMP) as black bands, marine temperature curve generalized from data in Kauffman (1977a).

Kauffman 1984

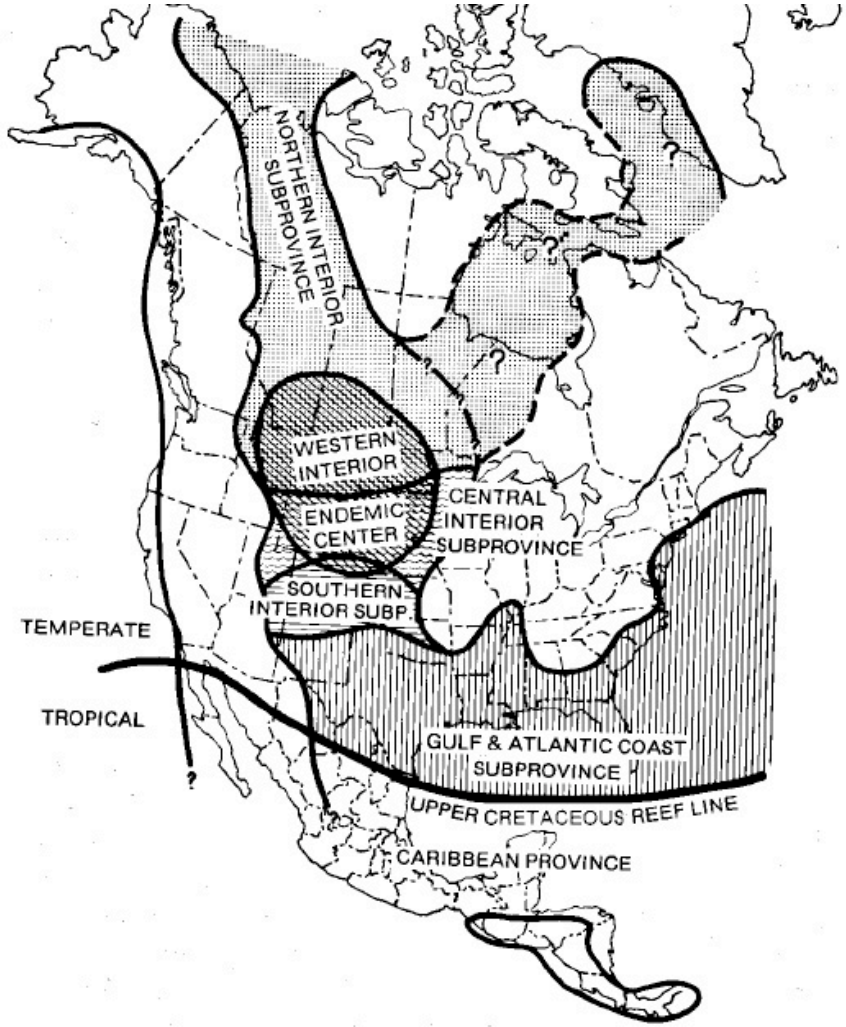

Figure 7. Generalized map of the Western Interior Cretaceous Seaway of North America, showing average distribution of paleobiogeographic units (Subprovinces, Provinces) during early to middle transgression and middle to late regression associated with all third-order tectonoeustatic cycles. Map also shows average extent of paleobiogeographic ecotone (endemic center), within which most rapid evolution took place. Subprovinces and provinces defined on percent molluscan endemism (10 to 25% and 25 to 50%, respectively). From north to south, subprovinces reflect Cool Temperate, Mild Temperate, Warm Temperate, and Subtropical climatic zones, as defined in modern American coastal settings by Hall (1964) and others.

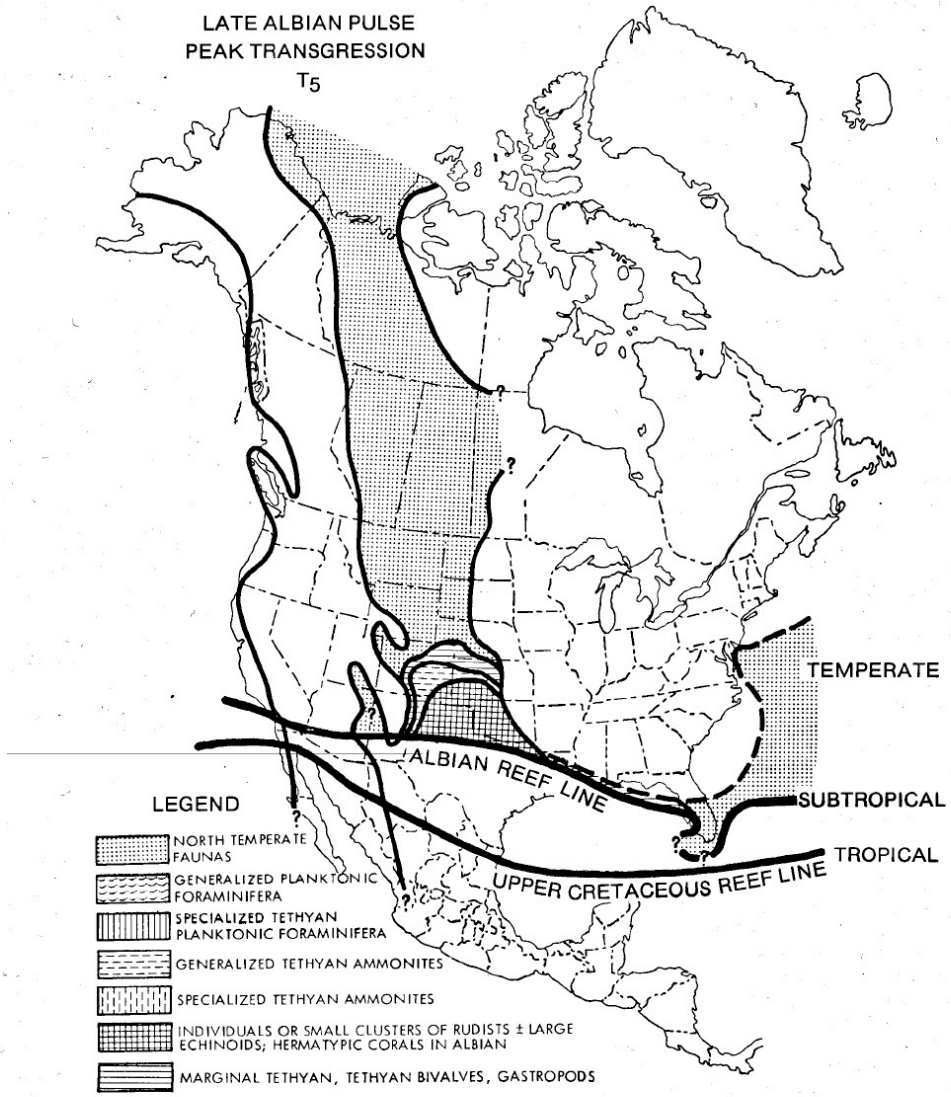

Figure 8. Generalized map of the Western Interior Cretaceous Seaway of North America during peak Late Albian transgression associated with the Kiowa-Skull Creek Eustatic Cycle. Map shows distribution of various Subtropical organisms (patterns keyed to lower left of diagram) defining northward shift of Temperate-Subtropical paleobiogeographic units during brief incursion of warm normal marine waters into the seaway at eustatic high-stand. Note in particular brief northward shift of Albian Tropical reef line from normal Upper Cretaceous position (heavy dark line). **Compare** with more normal paleobiogeographic distributions in **Figure 7.**

Kauffman 1984

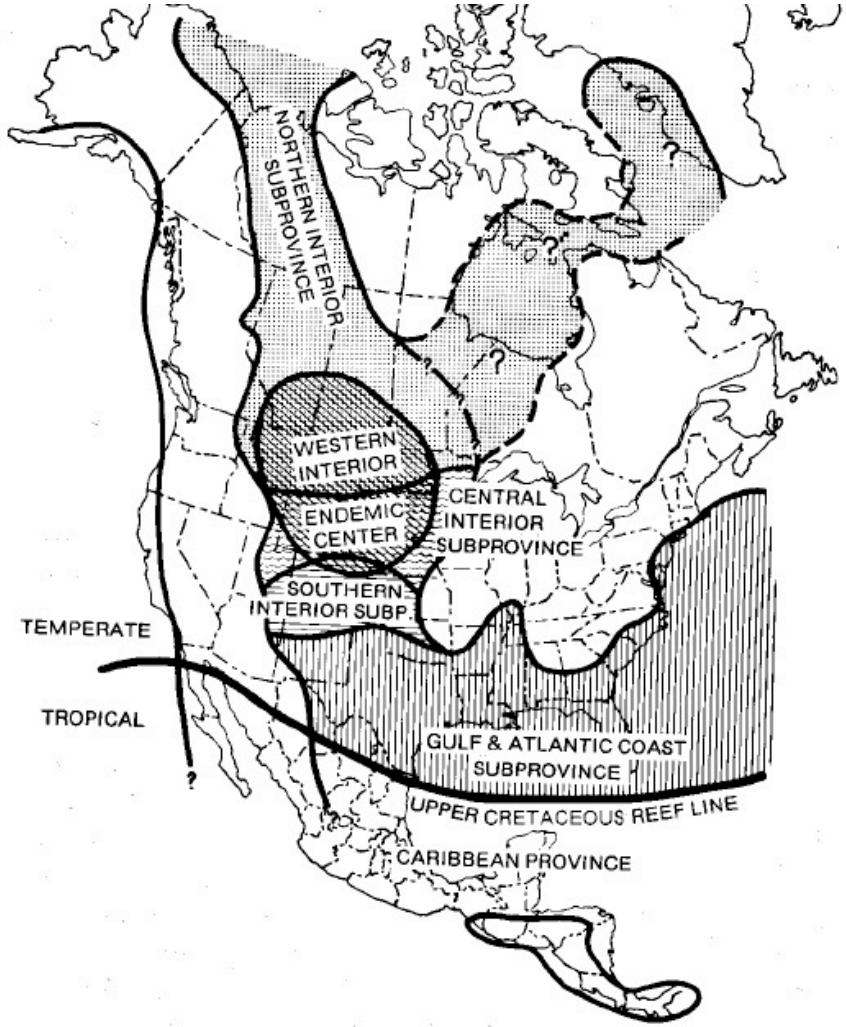

Figure 7. Generalized map of the Western Interior Cretaceous Seaway of North America, showing average distribution of paleobiogeographic units (Subprovinces, Provinces) during early to middle transgression and middle to late regression associated with all third-order tectonoeustatic cycles. Map also shows average extent of paleobiogeographic ecotone (endemic center), within which most rapid evolution took place. Subprovinces and provinces defined on percent molluscan endemism (10 to 25% and 25 to 50%, respectively). From north to south, subprovinces reflect Cool Temperate, Mild Temperate, Warm Temperate, and Subtropical climatic zones, as defined in modern American coastal settings by Hall (1964) and others.

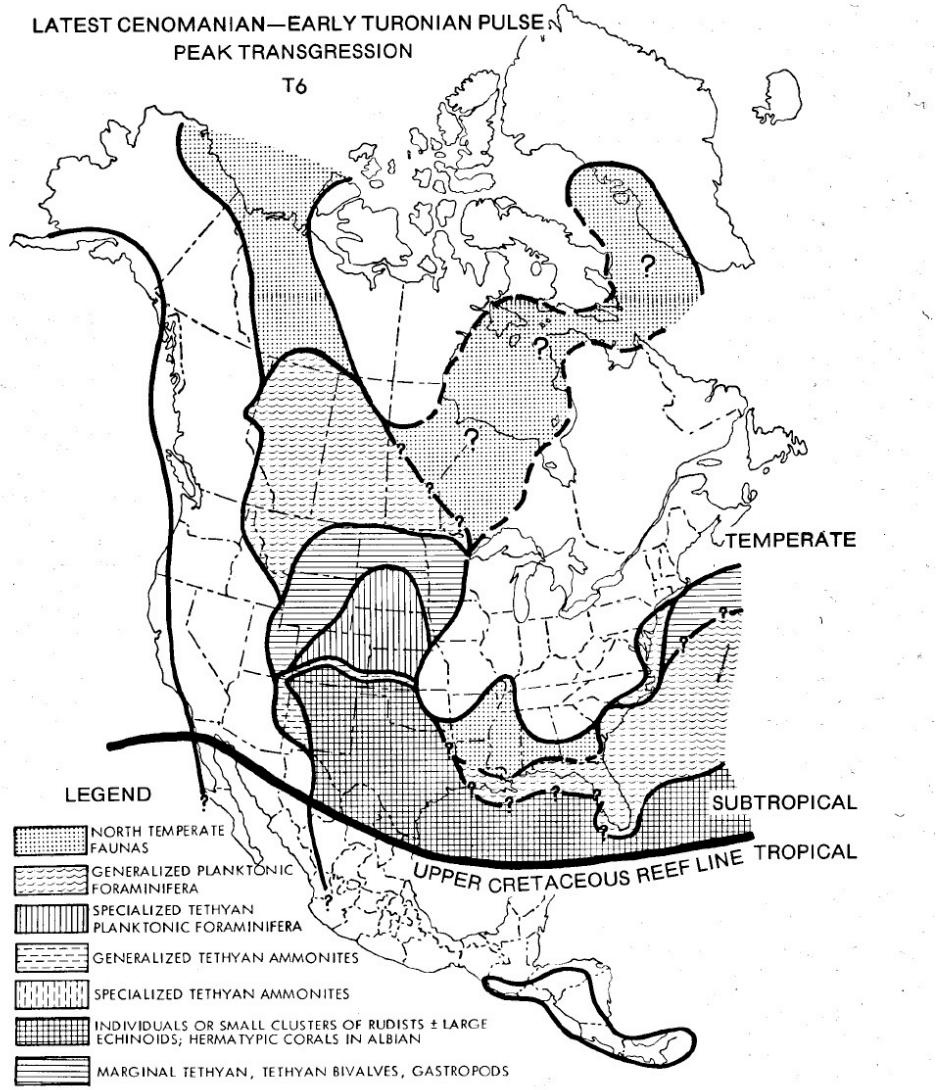

Figure 9. Generalized map of Western Interior Cretaceous Seaway of North America during peak Early Turonian transgression associated with the Greenhorn Eustatic Cycle. Map shows distribution of various Subtropical organisms (patterns keyed to lower left of diagram), defining extensive, short-term, northward migration of Warm Temperate and Subtropical paleobiogeographic units during rapid incursion of warm, normal marine waters into the seaway at eustatic highstand. Compare with more normal paleobiogeographic distributions in Figure 7.

Kauffman 1984

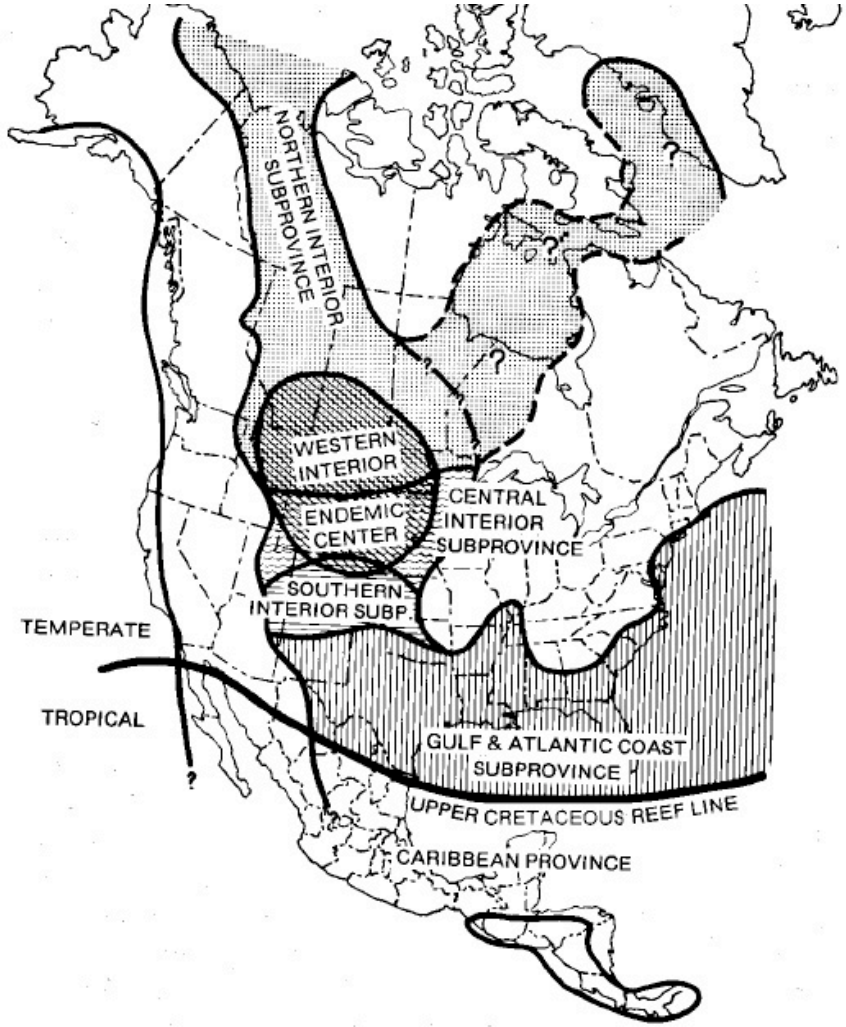

Figure 7. Generalized map of the Western Interior Cretaceous Seaway of North America, showing average distribution of paleobiogeographic units (Subprovinces, Provinces) during early to middle transgression and middle to late regression associated with all third-order tectonoeustatic cycles. Map also shows average extent of paleobiogeographic ecotone (endemic center), within which most rapid evolution took place. Subprovinces and provinces defined on percent molluscan endemism (10 to 25% and 25 to 50%, respectively). From north to south, subprovinces reflect Cool Temperate, Mild Temperate, Warm Temperate, and Subtropical climatic zones, as defined in modern American coastal settings by Hall (1964) and others.

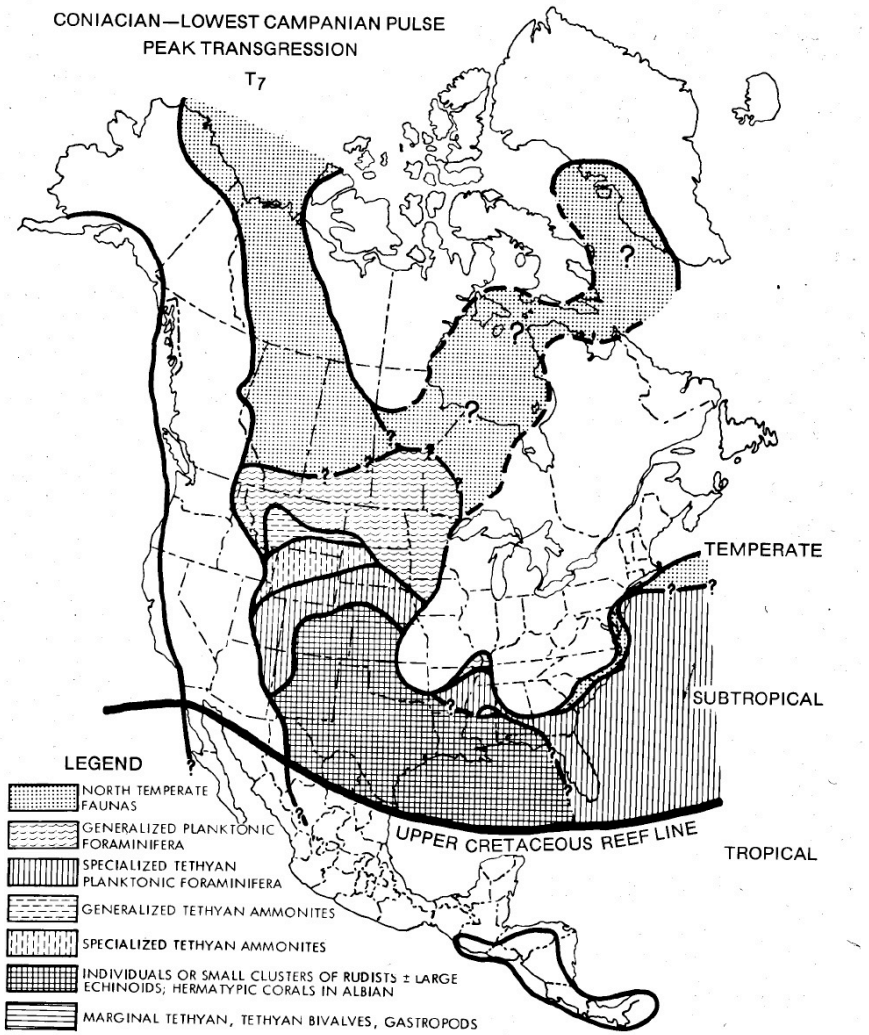

Figure 10. Generalized map of Western Interior Cretaceous Seaway of North America during peak Coniacian-Late Santonian fourth-order transgressions within third-order Niobrara Eustatic Cycle. Map shows distribution of various Subtropical organisms (patterns keyed to lower left of diagram), defining extensive, short-term northward migration of Warm Temperate and Subtropical paleobiogeographic units into the seaway during rapid incursion of warm, normal marine waters at eustatic highstand. Compare with more normal paleobiogeographic distributions in Figure 7.

Kauffman 1984

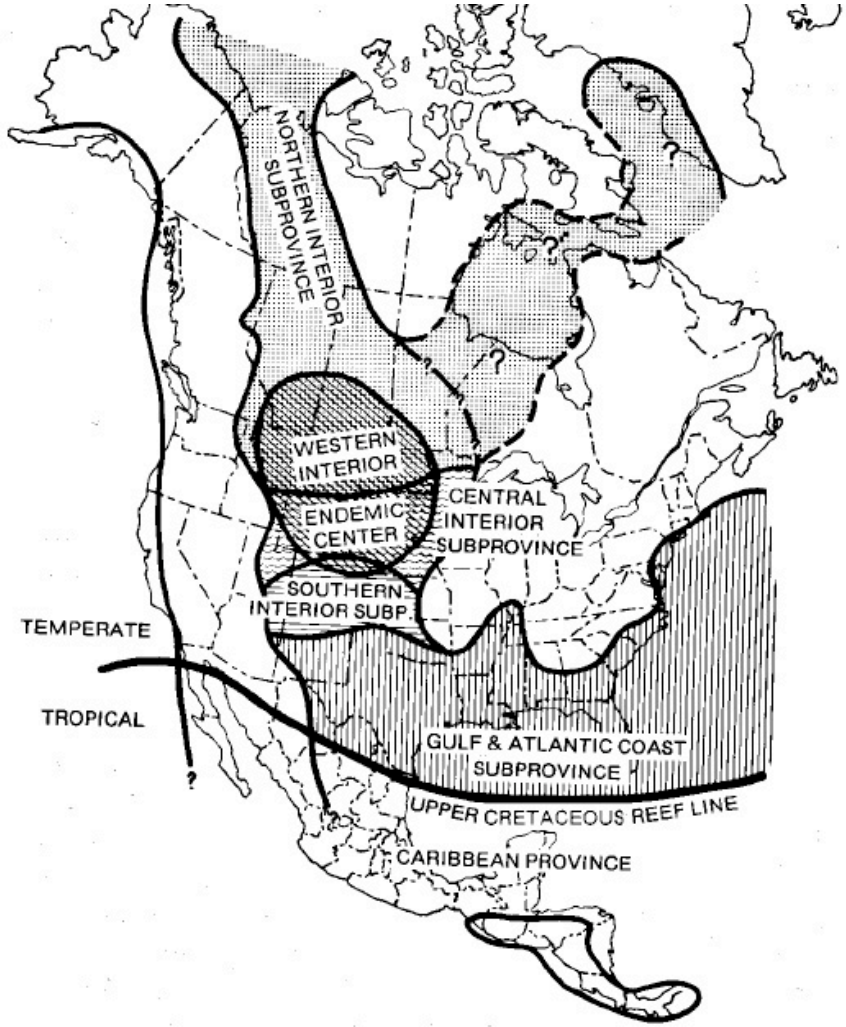

Figure 7. Generalized map of the Western Interior Cretaceous Seaway of North America, showing average distribution of paleobiogeographic units (Subprovinces, Provinces) during early to middle transgression and middle to late regression associated with all third-order tectonoeustatic cycles. Map also shows average extent of paleobiogeographic ecotone (endemic center), within which most rapid evolution took place. Subprovinces and provinces defined on percent molluscan endemism (10 to 25% and 25 to 50%, respectively). From north to south, subprovinces reflect Cool Temperate, Mild Temperate, Warm Temperate, and Subtropical climatic zones, as defined in modern American coastal settings by Hall (1964) and others.

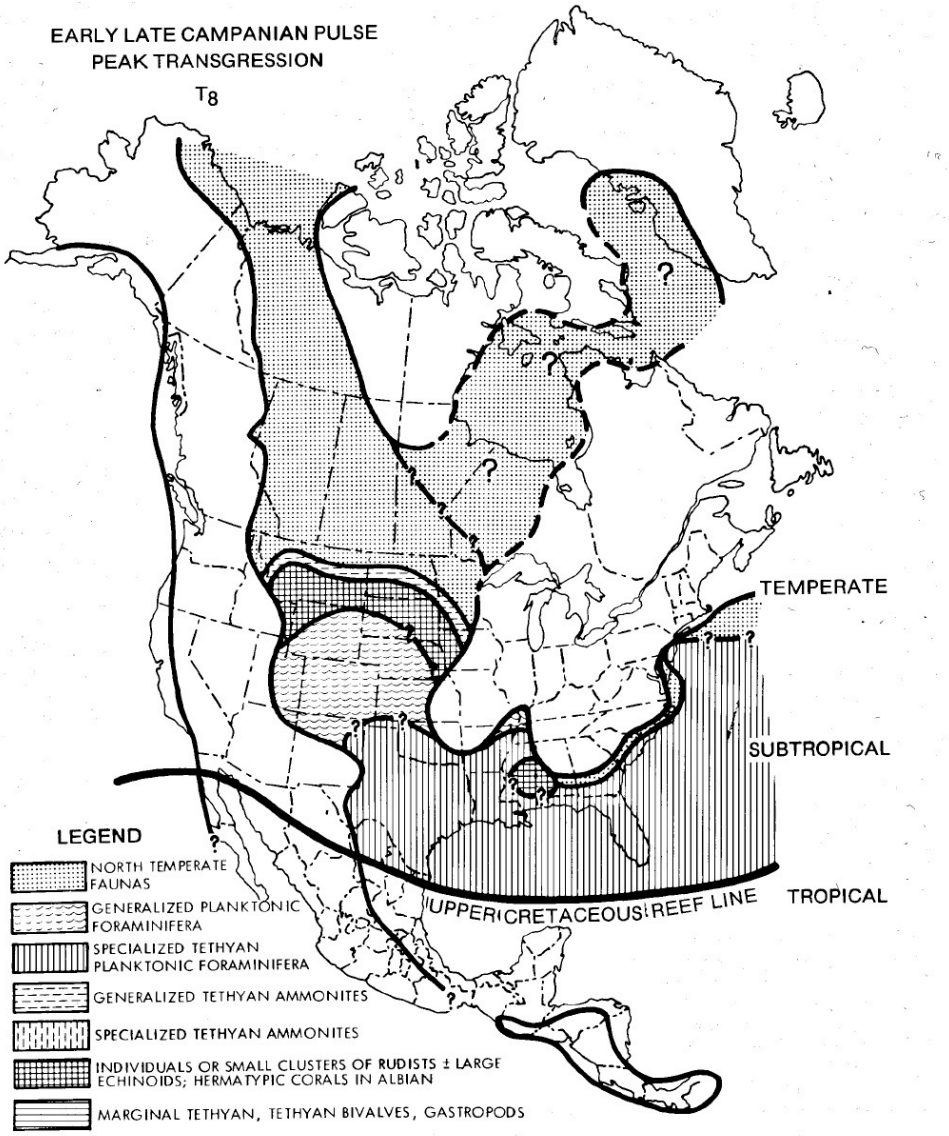

Figure 11. Generalized map of Western Interior Cretaceous Seaway of North America during peak early Late Campanian transgression associated with the Claggett Eustatic Cycle. Map shows distribution of various Subtropical organisms (patterns keyed to lower left of diagram), defining extensive, short-term northward migration of Warm Temperate and Subtropical paleobiogeographic units during rapid incursion of warm, normal marine waters into the seaway at eustatic highstand. Compare with more normal paleobiogeographic distributions in Figure 7.

Kauffman 1984

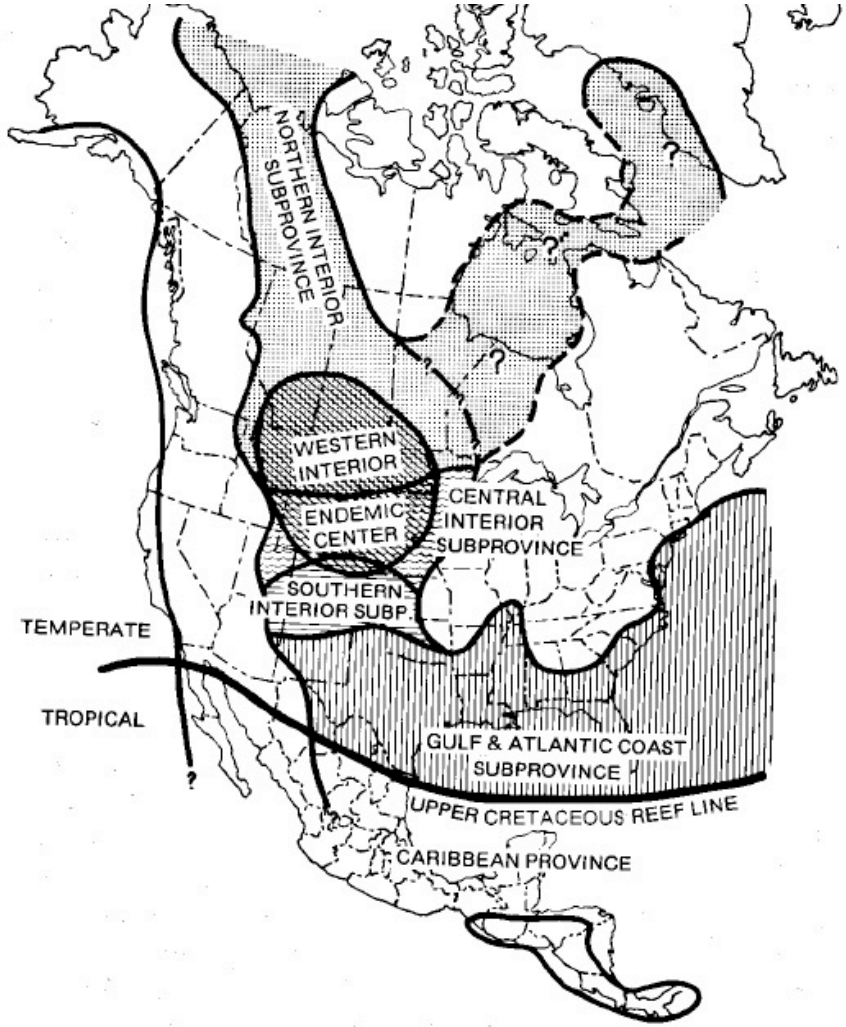

Figure 7. Generalized map of the Western Interior Cretaceous Seaway of North America, showing average distribution of paleobiogeographic units (Subprovinces, Provinces) during early to middle transgression and middle to late regression associated with all third-order tectonoeustatic cycles. Map also shows average extent of paleobiogeographic ecotone (endemic center), within which most rapid evolution took place. Subprovinces and provinces defined on percent molluscan endemism (10 to 25% and 25 to 50%, respectively). From north to south, subprovinces reflect Cool Temperate, Mild Temperate, Warm Temperate, and Subtropical climatic zones, as defined in modern American coastal settings by Hall (1964) and others.

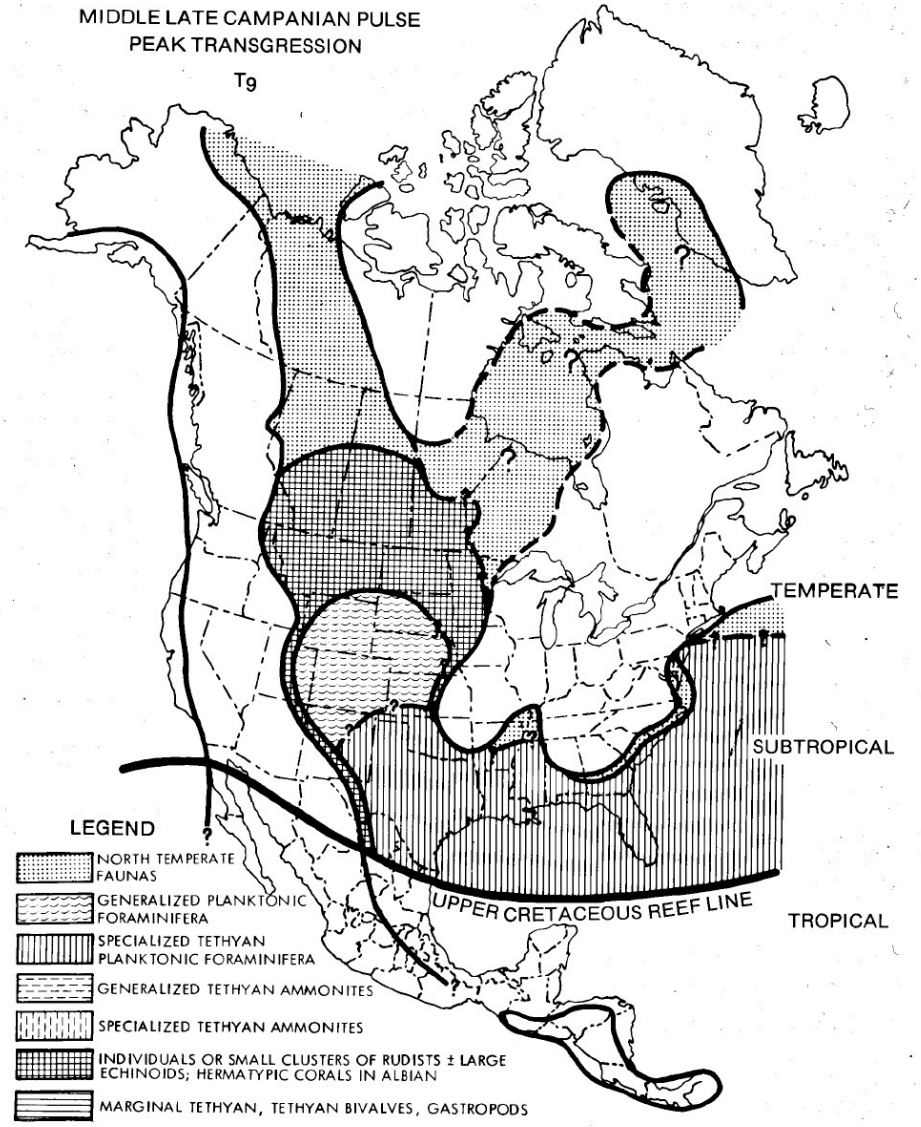

Figure 12. Generalized map of Western Interior Cretaceous Seaway of North America during peak middle Late Campanian transgression associated with the Bearpaw Eustatic cycle. Map shows distribution of various Subtropical organisms (patterns keyed to lower left of diagram), defining extensive, short-term migration of Warm Temperate and Subtropical paleobiogeographic units during rapid incursion of warm, normal marine waters into the seaway at eustatic highstand. Compare with more normal paleobiogeographic distributions in Figure 7.

Kauffman 1984

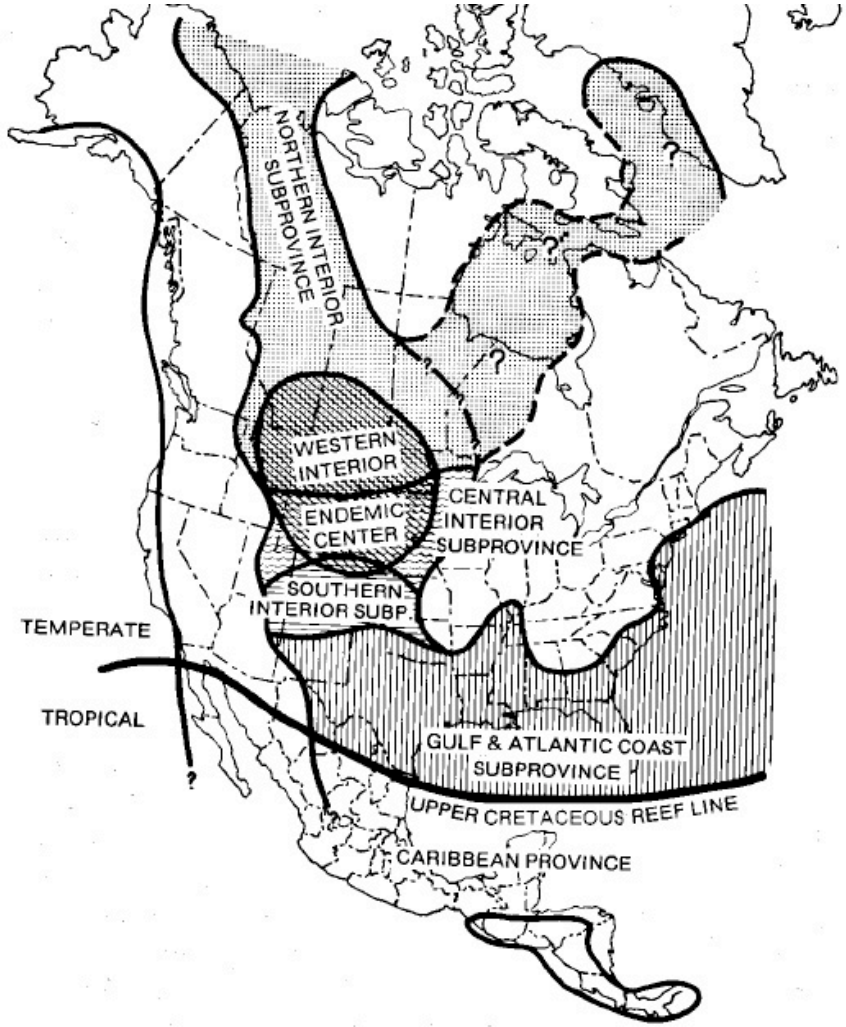

Figure 7. Generalized map of the Western Interior Cretaceous Seaway of North America, showing average distribution of paleobiogeographic units (Subprovinces, Provinces) during early to middle transgression and middle to late regression associated with all third-order tectonoeustatic cycles. Map also shows average extent of paleobiogeographic ecotone (endemic center), within which most rapid evolution took place. Subprovinces and provinces defined on percent molluscan endemism (10 to 25% and 25 to 50%, respectively). From north to south, subprovinces reflect Cool Temperate, Mild Temperate, Warm Temperate, and Subtropical climatic zones, as defined in modern American coastal settings by Hall (1964) and others.

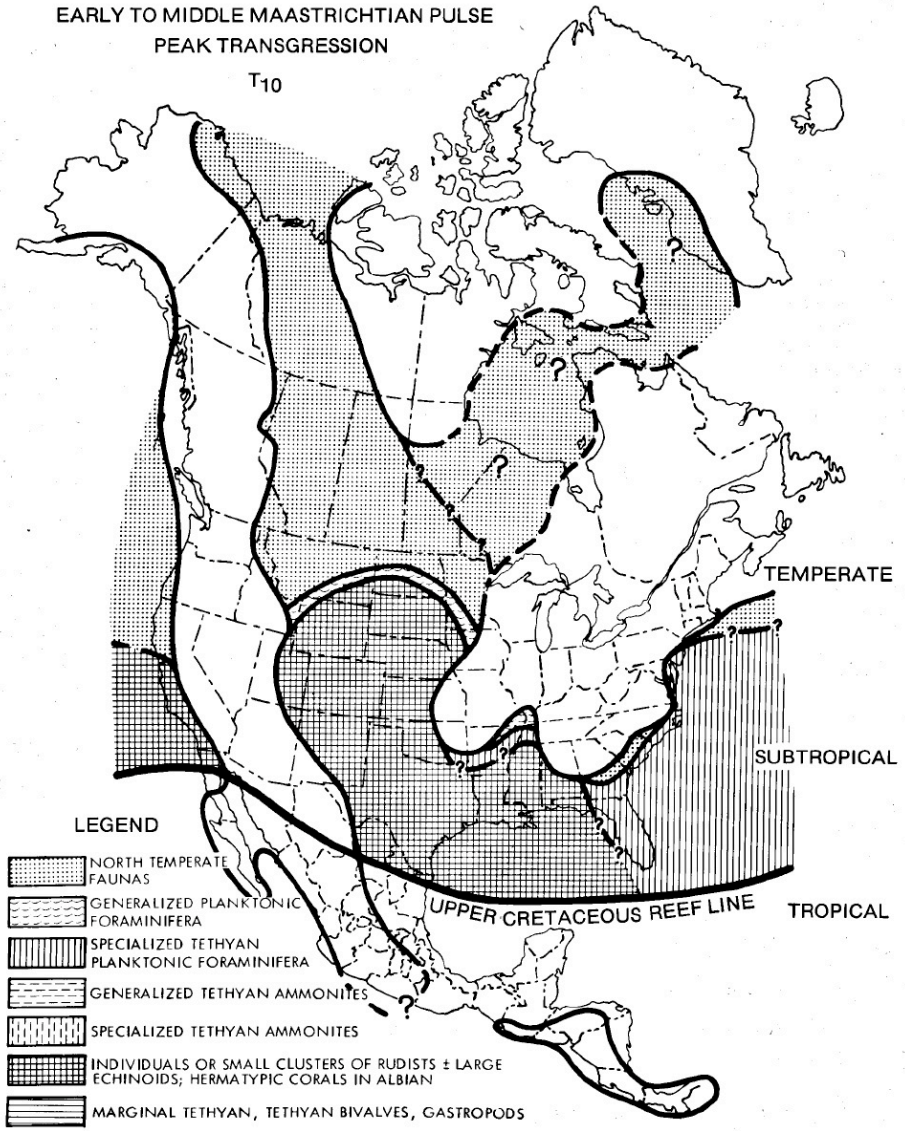

Figure 13. Generalized map of Western Interior Cretaceous Seaway of North America during a small Middle Maastrichtian eustatically-generated transgression associated with deposition of the Fox Hills Sandstone. Map shows distribution of various Subtropical organisms (patterns keyed to lower left of diagram), defining extensive, short-term migration of Warm Temperate and Subtropical paleobiogeographic units during rapid incursion of warm, normal marine waters into the seaway at small eustatic highstand. Compare with more normal paleobiogeographic distributions in Figure 7.

Kauffman 1984

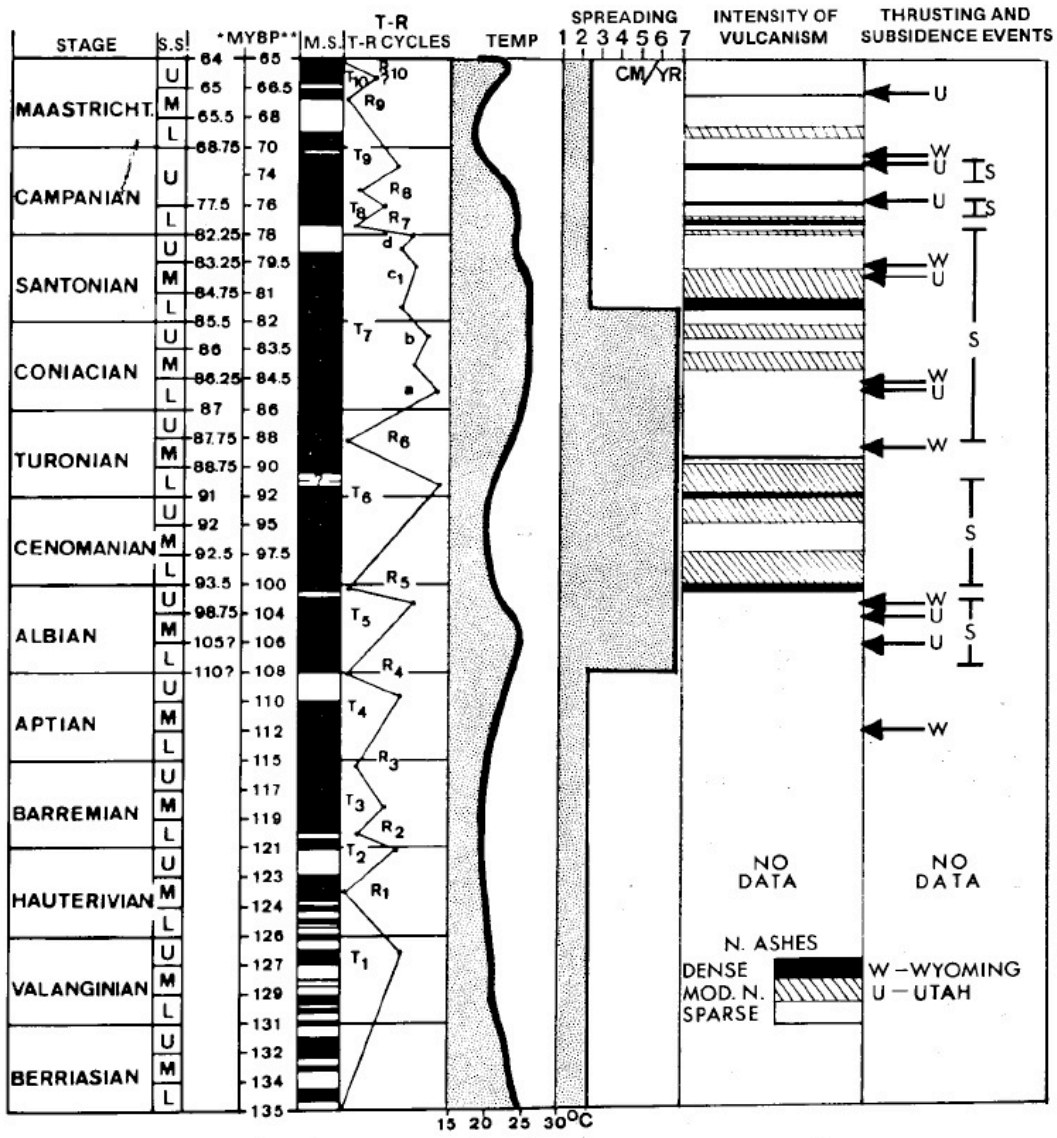

Figure 4. Geochronologic and magnetostratigraphic dating of global sealevel changes; third-order transgressive-regressive (T-R) epicontinental cycles (from Kauffman, 1977a); average marine temperature fluctuations (averaged from data in Kauffman, 1977a); Atlantic and Pacific half-spreading rates averaged (Larson and Pitman, 1972; Sheridan *et al.*, 1982); episodes of intense (black) and moderately intense (striped) volcanism, measured by number and magnitude of volcanic ash events (partially from Kauffman *et al.*, 1976); initiation of major thrusting (arrows) in Utah (U) and Wyoming (W) (data from Villien and Kligfield, pers. commun., 1984, and Wiltschko and Dorr, 1983, respectively); and times of most active basin subsidence (S), determined stratigraphically, in the Western Interior Seaway. Note correlation of active tectonism, subsidence, and volcanism with periods of active plate spreading and global sealevel rise, as contrasted to periods of relative tectonic quiescence during sealevel fall. Generalized time scales from Kauffman (Western Interior Seaway, left column, 1977a) and Van Hinte (global; right column, 1976).

Kauffman 1984

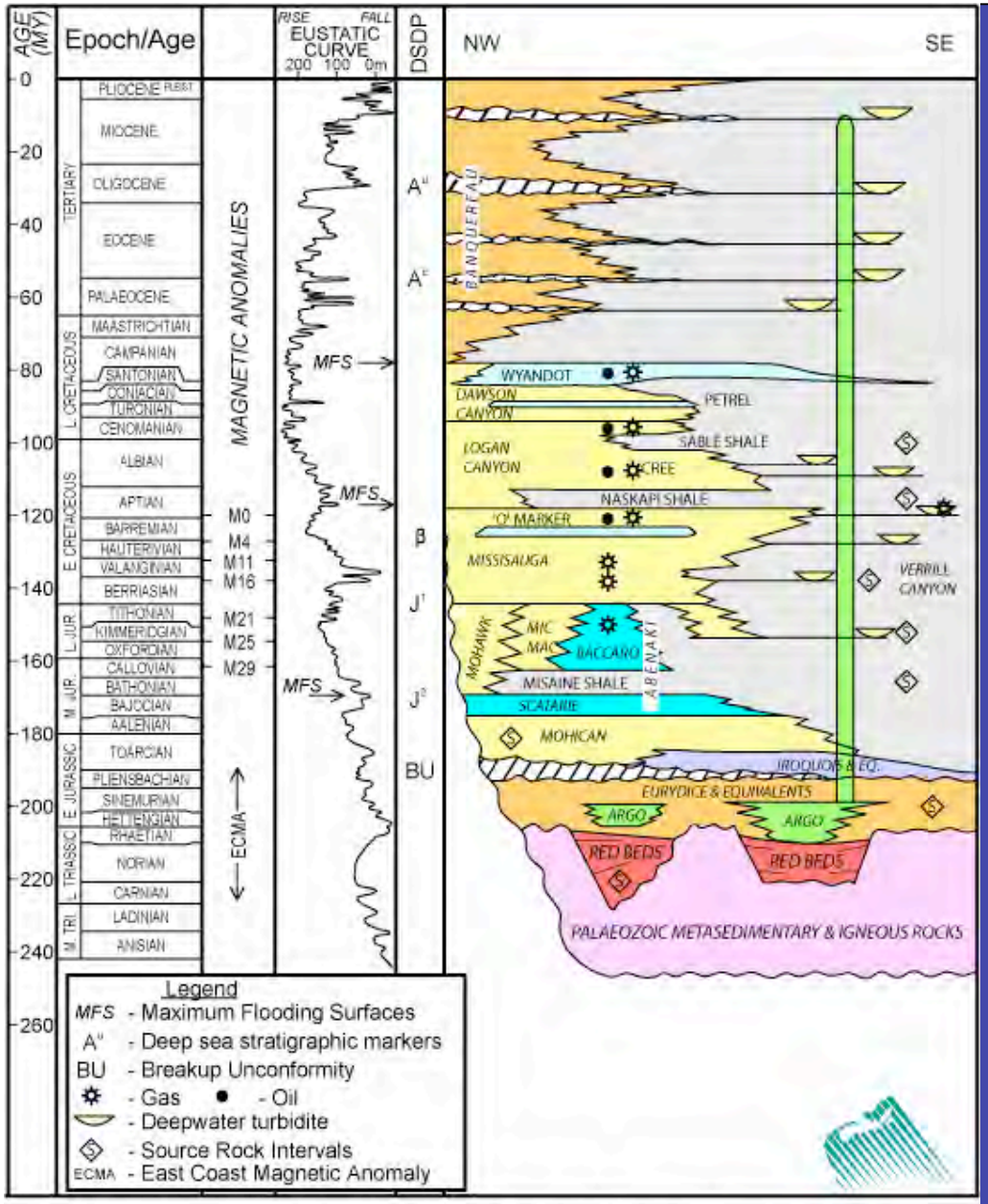

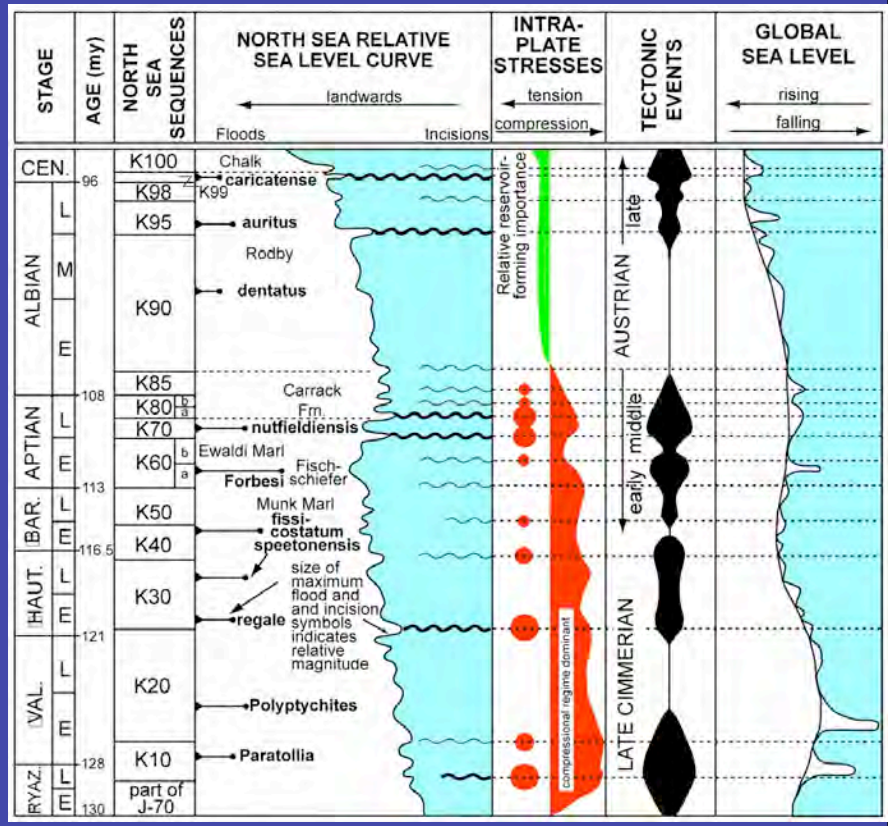

Figure 4: Generalized stratigraphic column for the Scotian Basin, offshore Nova Scotia (CNSOPB). Detailed columns can be found in Wade & MacLean, (1990). Sea level curve from Haq et al. (1987).

Newspaper Rock near Moab, Utah